Utrecht University

Carbon Deposits on Fluid Catalytic Cracking Catalyst Particles

Master thesis
Inorganic Chemistry and Catalysis
Debye Institute for Nanomaterials Science
Utrecht University

Rowie Frijsen
4277759
February 23, 2024

Under the supervision of
Robin Vogel Msc.
Caroline Versluis Msc.
Prof. dr. Eelco Vogt
Dr. Matteo Monai
2023-2024

Abstract

Fluid catalytic cracking (FCC) reaction is a refinery reaction which can convert low value feedstock to more valuable feedstock such as gasoline or diesel. For the cracking reaction a FCC catalyst is used. During this reaction carbon deposits on the catalyst particle, the coke species covers the active sites and blocks the pores. The catalyst will be in the reactor for ±5000 cycles, due to the interconnected reactors. This will lead to damage of the catalyst particles, and this results in a lower activity of the catalyst. Therefore, a part of the catalyst is removed from the reactor and fresh catalyst is added to reactor, this mixture of catalyst is called Equilibrium catalyst (Ecat). The formation of carbon deposits can be investigated with time-gated Raman spectroscopy and confocal fluorescence microscopy. To investigate this, *ex situ* and *in situ* experiments are performed with Ecat samples and fresh FCC catalyst (Fcat) with different amounts of coke species. The results of the confocal fluorescence microscopy of the Ecat shows an increase in the fluorescence intensity between 600 and 740 nm for an increasing exposure time of hexane. This means that there is a trend in smaller and larger coke species. A conventional Raman spectrometer is used to record the Raman spectra this is because the higher quality of the Raman spectrum compared to the time-gated Raman spectrum. However, the time-gated Raman spectrometer is used to study the dynamics of the fluorescence. The average fluorescence lifetime plot and the average spectrum of the *ex situ* measurements can be used to compare the different samples. The Ecat samples show the same trend for the average fluorescence lifetime, first an increasing average fluorescence lifetime followed by a decrease, with an increasing exposure of hexane. The average Raman spectrum shows an increasing RTR (%) for the samples with an increasing hexane exposure. The Fcat samples shows a different trend for the average fluorescence lifetime, first a decrease followed by an increase with an increasing hexane exposure. The *in situ* experiments are also performed with a combination of time-gated Raman spectroscopy and conventional Raman spectroscopy. The *in situ* measurements of Ecat show the same trends as the *ex situ* experiments. The RTR (%) of the Fcat samples of the *in situ* measurements show a different trend compared to the *ex situ* measurements. The fluorescence lifetime measurements and the Raman spectra give complementary information about the formation of carbon deposits on the FCC catalyst particle.

Layman abstract

Energy sources such as gasoline or diesel can be obtained through different refinery processes. One of the most used processes is Fluid catalytic cracking (FCC), with this reaction vacuum gasoil can be cracked into smaller molecules such as gasoline or diesel. For the cracking reaction a FCC catalyst is used. The FCC reactor contains two interconnected compartments, one for the cracking reaction and one for the stripping. The stripping reactor is used to remove the carbon deposits, formed as a by-product during the cracking reaction. Due to the interconnected reactors the catalyst can be used continuously. However, this can result in damage of the active site of the catalyst. Therefore, a part of the catalyst is removed from the reactor and fresh catalyst is added to the reactor. This results in a mixture of catalyst particles with different activities, this mixture is called Equilibrium catalyst (Ecat). To investigate in the formation of the carbon deposits different samples are prepared with a hexane cracking reaction. These reactions are performed with Ecat and fresh FCC catalyst (Fcat). The formation of the coke species is investigated with different techniques, time-gated Raman spectroscopy, conventional Raman spectroscopy and confocal fluorescence microscopy. Microscopy images of the different sample show a heterogeneous distribution of coke species over the sample, this is due to the different activities of the Ecat particles. The results of the confocal fluorescence microscopy show that there is a trend in smaller and larger coke species. Time-gated Raman can be used to determine the fluorescence lifetime of the coke species and conventional Raman can be used to obtain a Raman spectrum. These two techniques are combined during *ex situ* (measurement after the reaction) and *in situ* (measurement during the reaction) experiments to obtain both spectra of the sample particle. The average fluorescence lifetime and the average Raman spectrum of the particles can be used to compare the different samples. The *ex situ* and the *in situ* experiments of the Ecat samples shows the same trends for the average fluorescence lifetime and the average Raman spectrum. The average fluorescence lifetime of the Fcat samples shows the same trend for the *ex situ* and *in situ* measurements. Both *ex situ* and *in situ* experiments give complementary information about the formation of carbon deposits on fluid catalyst cracking particles.

Abbreviations

CFM	Confocal fluorescence microscopy
CCD	Conventional Raman spectroscopy
Ecat	Equilibrium catalyst
Fcat	Fresh FCC catalyst
FCC	Fluid Catalytic Cracking
PAH	Polycyclic aromatic hydrocarbons
TGA	Thermogravimetric analysis
TGRS	Time-gated Raman spectroscopy

Table of contents

1. Introduction

Nowadays global warming and additional problems such as a rising sea level is a huge problem. Experts and governments of countries all over the world are trying to minimize and control these environmental changes.[1,2] Also, the ran out of natural reserves of crude oil leads to a shift in the finding alternative energy sources. Therefore, a transition from fossil fuels to an alternative such as biomass derived fuels is still investigated.[3–5] Biomass derived fuels can be obtained in the same reactor as the fossil fuels, fluid catalytic cracking process (FCC), and with the same FCC catalyst.[6,7] Due to the change in the future of the FCC reactor it is important to investigate in the formation of coke species on the FCC catalyst.

The fluid catalytic cracking process is one of the most widely used applications for cracking feedstock into fossil fuels. During this reaction vacuum gas oil (VGO) and heavy gas oil (HGO) can be cracked into smaller fraction and more valuable products such as gasoline, diesel, and commodity chemicals such as propylene.[6,8–10] The catalyst used for the FCC reaction is a FCC catalyst, the most important component of this catalyst is the active component zeolite. During the cracking reaction coke will be formed as a by-product on the catalyst, this results in a significantly activity loss, due to the carbon that covers the active sites and blocks the pores. The cracking is performed in the FCC reactor, which contains two interconnected reactors, the riser reactor, and the regenerator.[6,11] Due to the interconnector reactors the catalyst can be used continuously. This results in damage of the catalyst particle and therefore an activity loss of the catalyst. To compensate for the activity loss of the catalyst, a part of the catalyst is removed from the reactor, and fresh catalyst is added. As a result of this an equilibrium catalyst (E-cat) is circulating in the FCC unit, consisting of new fresh catalyst and spent catalyst with a low activity. If the crude oil is in contact with the catalyst, the coke deposition starts in the first 0.15 s.[12] Therefore, chemical imaging of the formation of coke is challenging.

The future of the FCC unit is not cracking crude oils into smaller molecules used for fuels. The catalyst can also be used for cracking alternative feedstocks to obtain cleaner fuels.[7] Because of this it is important to investigate in the formation of carbon deposition on the catalyst. There are still several questions about the coke formation, such as where and how the carbon deposition starts first. To study the coke formation on the catalyst different techniques will be used, such as time-gated Raman spectroscopy (TGRS) and confocal fluorescence microscopy (CFM). The main goal of this research project is gaining insight the coking process with *ex situ* and *in situ* TG-RS and with CFM.

2. Theoretical background

2.1. Fluid catalytic cracking process

The fluid catalytic cracking process (FCC) is a refinery process that is used on large scale.[6,8,12] This reaction converts low value long chain feedstock such as vacuum gas oil (VGO) and heavy gas oil (HGO), to more valuable products such as gasoline, diesel or propylene.[6,8,13] The FCC cracking reaction is performed in the FCC reactor, shown in Figure 1. This reactor contains a regenerator and a riser reactor, which are interconnected to permit transferring the catalyst from the riser to the regenerator. Therefore, the cracking process can be continuous.[6,8–10] The cracking process in an endothermic process and the heat that is required comes from the pre-heated feedstock and the hot catalyst. The hot catalyst, from the regenerator, is combined with the feedstock in the riser reactor. This mixture is immediately transported to the top of the riser reactor, with a speed of 40 m/s.[6] Therefore, the contact time of the catalyst and the feedstock is only a few seconds, this means that the reaction also takes place in a few seconds.[12] At the top of the riser reactor, the catalyst and the products are separated. The spent catalyst is transported back to the regenerator, in this reactor the coke species that are formed during the reaction are burned off with hot air, this process is called the stripping.[11,14–16] Due to the interconnected reactors, the catalyst will be used continuously, this can result in damage of the active sites of the catalyst particles. A catalyst particle is around 5000-cycles in the reactor.[17] Due to the thousands of cycles, the catalyst particles are damaged, and this will lead to an activity loss of the catalyst. To compensate for this activity loss, a part of the catalyst is removed from the regenerator and fresh catalyst is added. This results in a mixture of spent catalyst with a low activity and fresh catalyst with a high activity, this mixture is called equilibrium catalyst, E-cat.

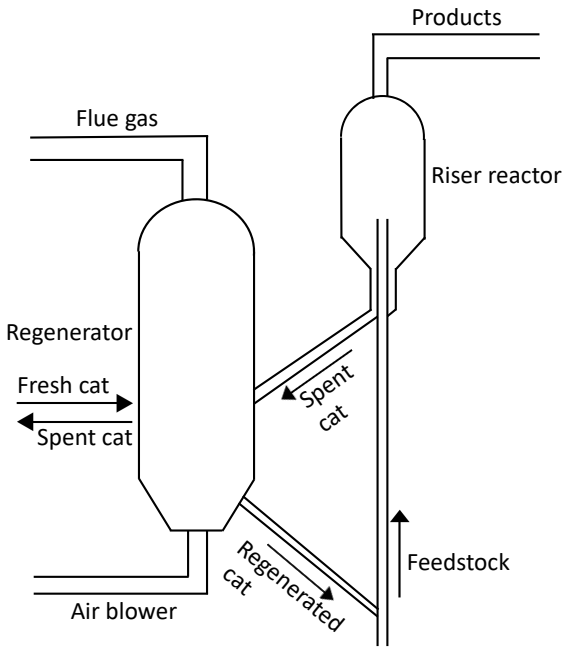

Figure 1: *Schematic view of a Fluid Catalytic Cracking (FCC) reactor.*[11,14]

2.1.1. Catalyst particle

The FCC reaction is performed with a fluid catalytic cracking catalyst particle, the catalyst particle is around 60-80 µm.[6,10] A catalyst particle contains different materials, such as zeolite, alumina and silica (matrix), filler, binder and metal traps (Figure 2). The zeolite is the main active component of the catalyst particle, usually zeolite Y is used.[6,8,10] Zeolite Y is a highly active zeolite, which results in a reaction time of only a few seconds.[8] Zeolite Y has an internal pore structure with Brønsted acid site and Lewis acid sites.[18] These acid sites facilitate the cracking of larger molecules into smaller molecules. The long chain feedstock cannot enter the pore structure of the zeolite. The meso- and macro pores in the matrix are used as a pre-cracking, due to the acid sites of the alumina and silica.[6,11] The long chain feedstock can enter these pores and can be cracked into smaller molecules, who can enter the pores of the zeolite. The clay is only the filler of the catalyst, and the binder is the glue to bind everything together.

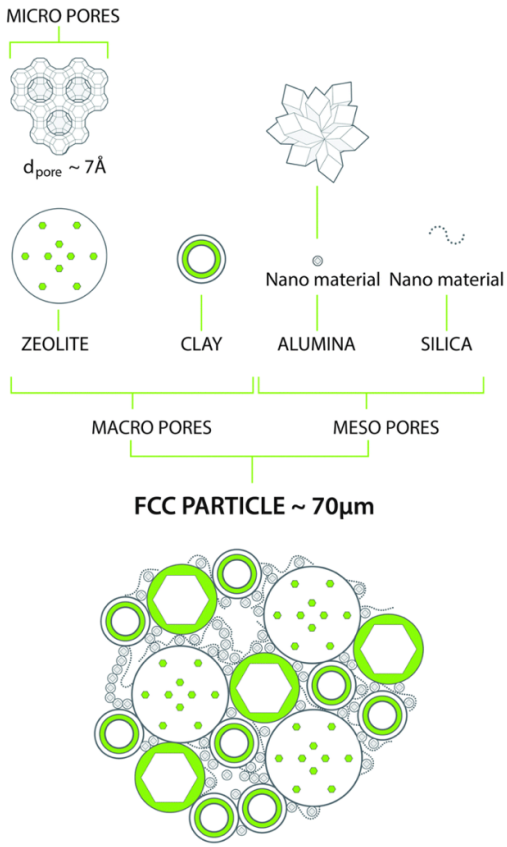

Figure 2: *Chemical and structural composition of a Fluid Catalytic Cracking Catalyst particle. Adopted from vogt et al. 2015.*[6]

2.1.2. Alternative feedstock

Due to environmental issues, the running out of reserves of crude oil, and stringent government rules about these environmental issues. There is a shift in finding alternative energy sources. One of those alternative energy sources can be biomass derived feedstock.[7,10,19] The biomass derived feedstock produces less greenhouse gasses compare to fossil fuels.[7] During the cracking reaction of biomass derived feedstock there will be an increased amount of water and also a higher amount of carbon deposits on the catalyst. These coke species can be converted into synthesis gas (CO and H_2), this can be used at different reaction in the oil refinery.[6] Therefore, it is important to investigate in the formation of coke species on the FCC catalyst.[10]

2.1.3. Cracking process

The cracking reaction takes place on the surface of the catalyst, via a positively charged carbenium ion. The carbenium ion can be created via three different pathways, illustrated as reactions 1-3 in Figure 3.[6] In the first reaction a Brønsted acid sites donates a proton to an alkene, this alkene is already formed by thermal cracking. In the second pathway a Lewis acid sites or the Brønsted acid site can abstract a hydride from an alkane. The last pathway is that the Brønsted acid site donates a proton to an alkane and forms a carbonium ion. This carbonium ion can be transformed to a carbenium ion via protolytic cracking. The carbocations are formed at the active sites of the catalyst particle. The primary cracking reaction is the β -scission reaction, the beta C-C bond will break to the carbon with a positive charge, so a new carbocation and an olefin are obtained, reaction 4 in Figure 3. The new carbenium ion can further react with another alkane. The reaction stops when the carbocation bonds with a donor hybride or if the carbocation loses a proton. [6,8,20]

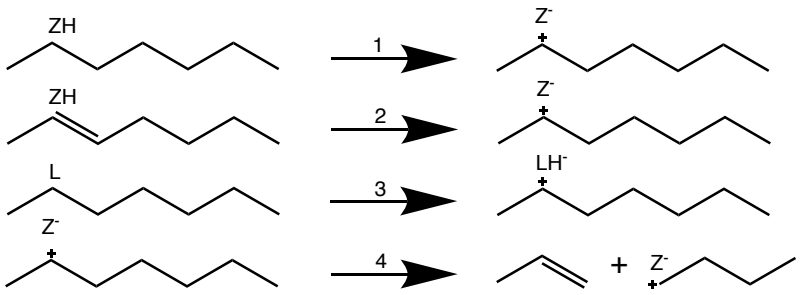

Figure 3: *Reaction 1-3, different pathways of the formation of a carbenium ion. Reaction 4: beta scission of a carbenium ion to a new carbenium ion and an alkene.*[6]

2.1.4. The formation of coke species

During the FCC reaction, a mixture of carbon deposits on the catalyst, this mixture is called coke. Different types of coke species are formed during the FCC reaction. The first type of coke species are the coke species deposited during the cracking reaction; mechanism is shown in Figure 4.[6,20] These coke species are formed as a by-product during the cracking and pre-cracking of the feedstock. This type of coke species is centered at the active sites of the catalyst particle and are formed in the first 0.15 s if the feedstock is in contact with the catalyst particles.[12] The second type of coke species is formed with unwanted dehydrogenation reactions on deposited poisoning metals. The third type of coke species are aromatic coke species from the feedstock.[8,10,20,21] These type of coke species deposit on the surface of the catalyst particle. All these different types of coke species result in deactivation of the catalyst particle because the coke species blocks the pores and covers the active sites of the catalyst particles. Therefore, it is important to investigate in the formation of coke species and obtain more information about the different stadiums of smaller and bigger coke species.

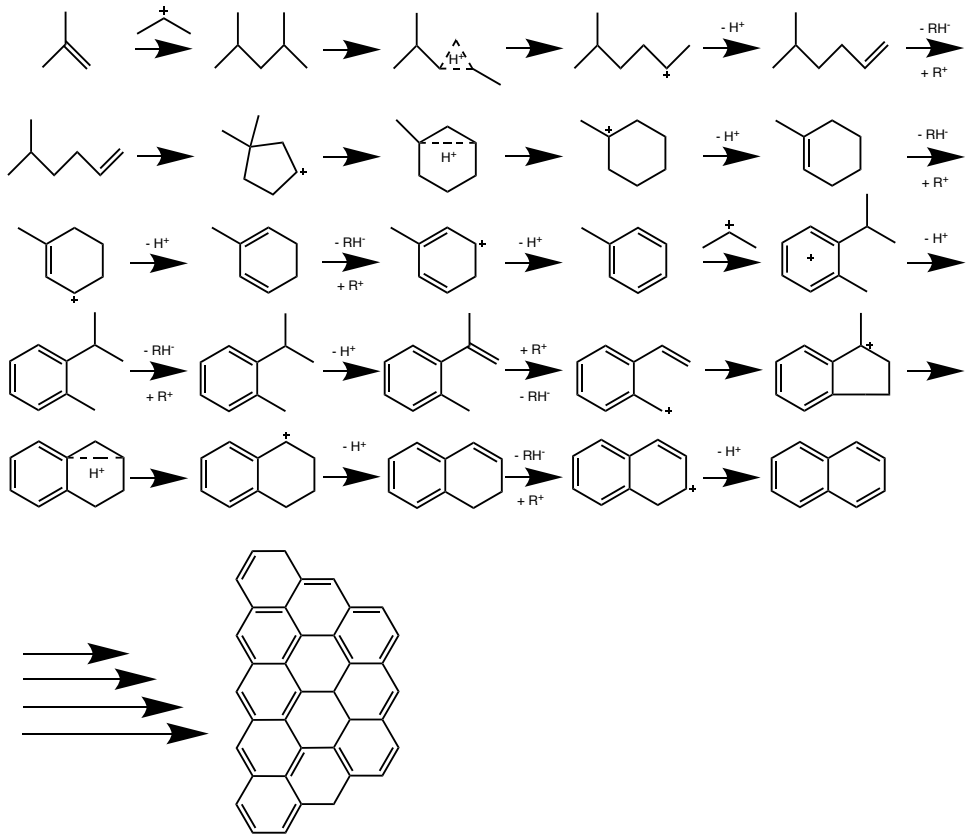

Figure 4: *The mechanism of the formation of coke species during Fluid Catalytic cracking process. Adapted from Vogt et al. 2023.*[20]

As shown in the mechanism of the formation of the coke species during the cracking reaction, coke species are polycyclic aromatic structure (PAH). These PAHs are formed from smaller to larger molecules and will form graphene structures. A lot of research is done of PAHs, because PAHs are carcinogenic and have mutagenic properties.[22,23] The information of the experiments of these PAHs can be used for the determination of different coke species formed at the catalyst particle.[22,24–26]

2.1.4.1. Polycyclic aromatic hydrocarbons

Polycyclic aromatic hydrocarbons (PAHs) are well defined cutouts of graphene. PAHs are built up by aromatic rings of six sp^2-hybridized carbon atoms.[27] The smallest PAH is benzene (one ring). The optical properties can give information about the structure and the size of the PAHs.[28] E. Clar has developed an easy system to estimate the stability of the PAHs, which is called the Clar's sextet rule.[28] The π-electrons of a PAH can be grouped in sextets, within one ring, this can be marked with a ring in the aromatic cyclic structure, illustrate in Figure 5A. According to Clar's sextet rule the electron sextets possess particularly strong aromatic stabilization. The bonds that are not in the sextet leads a smaller optical band gap.

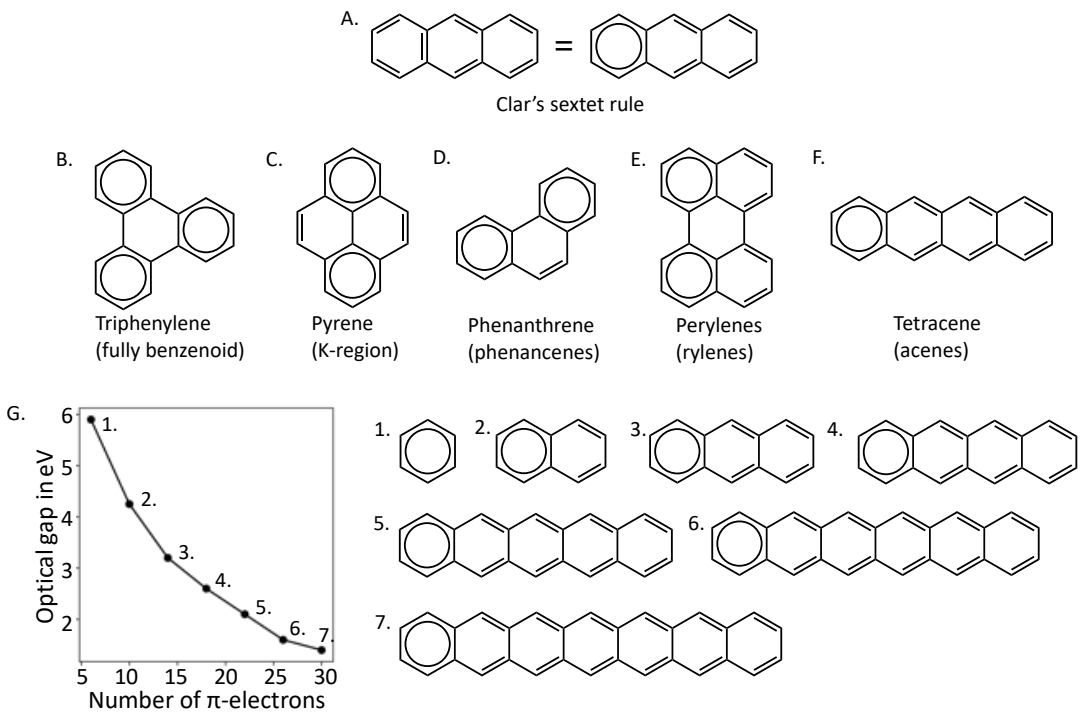

Figure 5: *A. example of Clar's sextet rule, π-electrons grouped in sextet, B-F. one example of each group of Clar's sextet groups, G. Example of optical band gap against number of π-electrons of the phenacenes group.*

According to Clar's rule, PAHs can be grouped into different groups, the structure of the PAH depends on the group of the molecule. The first group is the fully benzenoid PAHs, shown in Figure 5B, this group has the highest stabilization energy. This is because all the π-electron can be grouped into sextets. Research has shown that bigger fully benzenoid PAH results in a lower band gap and therefore a red shift of the fluorescence band.[28] In this group the optical band gap is almost unaffected by the different shapes of isomers.

The second group of the Clar sextets rule is called the K-region, an example is shown in Figure 5C. If an extra aromatic ring is added in a bay-region to a fully benzenoid PAH, the two outer π-electrons are not part of a sextet, this outer bond is less stabilized. One of the most common k-region PAHs is pyrene, pyrene has four aromatic rings and compared with a fully benzenoid PAH with four aromatic rings, the fluorescence signal of pyrene is red shifted. This means that outer π-electrons also result in a red shift of the fluorescence signal compared to the fully benzenoid.[28]

Other three groups are phenacenes (zigzag PAHs), rylenes (most common naphthalene) and acenes (linear PAHs), examples are shown in Figure 5D-F. All the three groups have a lower stability compared to the fully benzenoid PAHs. For rylenes and acenes, an increasing amount of aromatic rings results in a high red shift of the fluorescence signal. For phenacenes, the difference in aromatic stabilization is more important compared to an increasing number of aromatic rings. But also, this group has a small red shift of the fluorescence signal.[28] An example of the optical gap against the number of π-electrons is illustrated in Figure 5G. This example is from the acene group (linear PAHs). This graph show that the optical gap will be lower with an increasing number of π-electrons.

2.1.4.2. *Fluorescence lifetime*

When a molecule absorbs a photon of a certain energy, the molecule is excited to the excited state. The excited molecule can lose its energy via the emission of a fluorescence photon, this is called the relaxation. In fluorescing, the molecule may then go to various vibrational levels of the ground electronic state, as depicted in Figure 6.[29,30] The radiative relaxation occurs with a certain probability and a specific radiative decay rate (k). The average length of time that a fluorophore remains in the excited state is called the fluorescence lifetime (τ).[31,32] The fluorescence lifetime is a unique property of a fluorophore. The fluorescence lifetime is not dependent on, the wavelength of the excitation source and the duration of the light. The fluorescence lifetime is also independent of the concentration of the fluorophore. However, the fluorescence lifetime is dependent on external factors such as, the temperature, the medium and the polarity.[29,31,32]

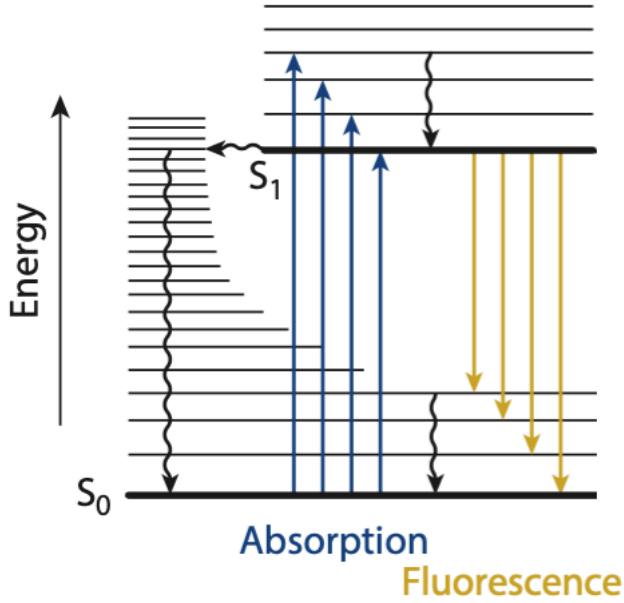

Figure 6: *Jablonski diagram showing the relation between absorption and fluorescence. Adopted from Maris et al. 2023.*[62]

$$\frac{1}{\tau_n} = 2.880 * 10^{-9} n^2 < \nu_f^{-3} >_{Av}^{-1} \left(\frac{g_l}{g_u}\right) \int \varepsilon(\nu) d\mathrm{In}\nu \qquad (1)$$

The fluorescence lifetime can be estimated with the Strickler-Berg equation, equation 1.[29,31] n = *refractive index*, ε =*molar absorptivity absorption spectra*, $< \nu_f^{-3} >_{Av}^{-1} = \nu_f^3$ is *fluorescent maximum* (cm^{-1}), and $\left(\frac{g_l}{g_u}\right)$ are the degeneracies of the lower and the upper states and is equal to $\left(\frac{g_l}{g_u}\right)$=1 for fluorescence transition. To use this equation several assumptions, have to be made, one of the assumptions is that: 'the absolute rigidity of the molecule in both the ground and excited state'.[31] This is difficult to achieve in real experiments, so the calculated value is different compared to the actual value. Therefore, the Strickler-Berg equation can be used as a screening tool for the fluorescence lifetime of different components. However, a lot of researchers have investigated the fluorescence lifetime of PAHs.[24–26,33] Most of them investigated only small PAHs (1-4 aromatic rings) and small PAHs cannot be excited with a 532 nm laser, used in this thesis, due to an absorption spectrum in a lower spectral range. Coke

species are mostly larger PAHs with more graphitization. Also, most researchers do not investigated PAHs from one group, defined by Rieger et al. The medium of the PAHs is also dependent on the fluorescence lifetime. Therefore, it is very challenging to find a trend in the literature values of the fluorescence lifetimes reported for different PAHs. This means that the fluorescence lifetime can only be related to the Clar's sextet rule and the red shift of the fluorescence signal. The red shift of the fluorescence signal of the PAHs has an influence on the fluorescence lifetime of the coke species. The fluorescence lifetime will increase if the small coke species (benzene) becomes larger. However, during the fluorescence lifetime measurements also the Raman scattering is measured. If the larger coke species become more graphitic, the fluorescence signal will decrease. This results in a decrease of the fluorescence lifetime. Therefore, the expectation is that the formation of the cokes species will results in an increase of the fluorescence lifetime followed by a decrease.

2.2. Raman spectroscopy

Raman spectroscopy is a vibrational spectroscopy technique which can provide information about the chemical structure, morphology, and crystallinity of a molecule.[34] During Raman spectroscopy monochromatic light is used for irradiation of the sample. This results in three different types of scattering, shown in Figure 7. Rayleigh scattering occurs when the frequency of the light is the same as the scattered light. The second type is that there is a change in the energy between the incident light and the scattering light. If the photon gains vibration energy of the molecule, it results in scattering light with a higher energy, and this is called anti-Stokes Raman scattering. The last type is that the molecules gain energy from the incident light, so the frequency of the scattering light is lower compared to the incident light. This process is called Stokes Raman scattering.[35–37]

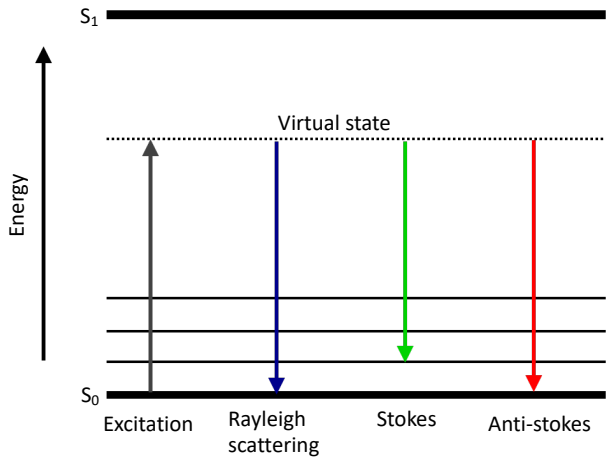

Figure 7: *Schematic view of different types of scattering during Raman spectroscopy, Rayleigh, Stokes and Anti-stokes scattering.*

Raman scattering is a weak signal, only one Raman photon is inelastically scattered from around 10^7 laser excited photons.[38] Therefore, a high laser power will increase the intensity of the Raman signal. Other factors can also have an influence on the quality of the Raman signal, such as the sensitivity of the detector. But also, blackbody radiation and the fluorescence signal of the sample. To reduce the fluorescence signal, a background correction can be used to obtain a more representative Raman spectrum.[35,39] However, random noise

cannot be subtracted and therefore the Raman spectrum has a higher amount of background counts.[40] Another option to reduce the fluorescence signal is using different types of lasers. For Raman measurements, lasers in visible light, near-IR (NIR) and UV can be used. The wavelength of the excitation laser has an influence on the intensity of the Raman scattering and on the intensity of the fluorescence signal. Using an excitation laser of visible light (400 – 600 nm) results in high Raman scattering but also in high fluorescence signal.[39] UV excitation (200-300 nm) can be used to avoid background fluorescence in the Raman spectrum.[41] If a laser of 200 nm is used, the Raman scattering occurs at between 200 and 208 nm and the fluorescence signal of PAHs is typically between 350-600 nm.[28] NIR excitation can also be used for Raman scattering, however this requires longer acquisition times and greater accumulation numbers.[42] This is because the Raman scattering is proportional to the λ^{-4} (λ is laser wavelength), so this will result in less intense Raman scattering. NIR excitation laser will result in less fluorescence signal, however this laser can increase the risk of sample damage.[41]

The Raman spectrum can be used as a 'fingerprint' of the sample. The spectrum of coke species shows two characteristic bands. The first band is around 1300 cm^{-1}, this band is called the D band. The D band is from the vibrations of the disordered graphite lattice and the edges of the coke species. The other band is around 1600 cm^{-1}, this band is called the G band. The G band is characteristic for the vibrations of the graphitic coke species, Figure 8 illustrates a Raman spectrum with a D and G band.[43–46] It is also possible that the Raman spectrum is dominated by the fluorescence signal, this results in a very broad band, sort of bump in the spectrum, around 1200-1600 cm^{-1}.[47,48]

To compare the Raman spectra of different particles, the Raman to Total ratio can be used.[49] For this calculation the Raman counts of the G band and the Raman counts of the background signal are subtracted and then divided by the background counts, this is called the RTR (%). This can give an indication of the graphitization of the sample, a higher RTR is due to less fluorescence background counts. Less fluorescence background means that there are more graphitic coke species because these graphitic coke species has less fluorescence. The degree of graphitization of the sample can also be determined by the ratio between the D band and the G band. This can also be used to compare the different samples.[45]

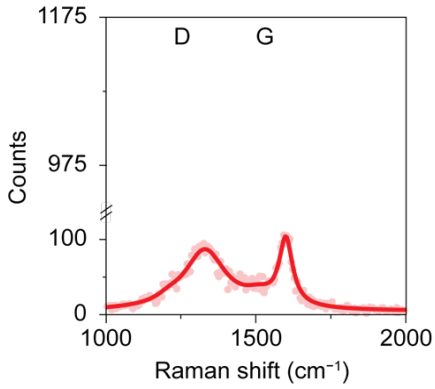

Figure 8: *Example of Raman spectrum of coke species with D and G band.*

2.2.1. Time-gated Raman Spectroscopy

Another solution of reducing the fluorescence signal is using time-gated Raman spectroscopy. The fluorescence signal which masks the weak Raman scattering can be partially suppressed, by using a pulsed laser and time-gated detection, illustrated in Figure 9A.[39,40,50] The aim of time-gated Raman spectroscopy is to increase the signal-to-noise (SNR) of the Raman spectrum, illustrated in Figure 9B. The Raman scattering has a very short lifetime due to the virtual state. However, the lifetime of the fluorescence signal is longer due to the real electronic exited state, Figure 9A. Therefore, the Raman and fluorescence signal can be separated in temporal domain.

The SNR can be maximized by tuning the width and the position of the time-gate. It is important that the laser pulse has a full width half maximum (FWHM) in picoseconds and that the detector is only activated during the emission pulses.[39,40,50] If the gating time is very short, neither the Raman signal nor the fluorescence signal will be detected. With a long gating time, all the fluorescence signals and the Raman signal will be detected. The fluorescence signal has the longest decay, so it is the easiest to cutoff. However, complete rejection of the fluorescence signal is not possible due to the fast rise of the fluorescence signal.[50]

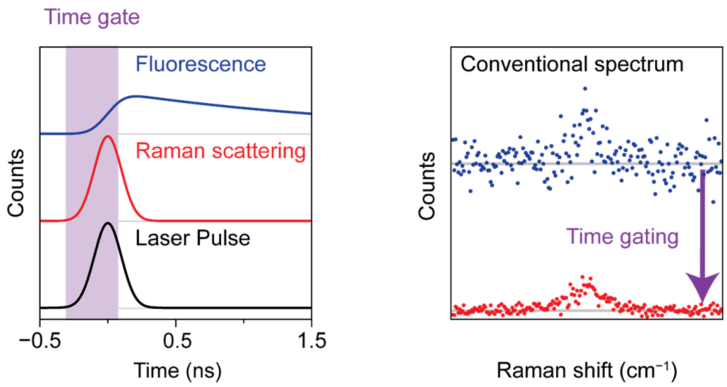

Figure 9: *A. Theory of Time-gated Raman spectroscopy, B. Lower background counts in the Raman spectrum recorded with the time-gated Raman spectrometer compared to the conventional Raman spectrometer. Adopted from Vogel et al. 2023.*[40]

2.3. Confocal fluorescence microscopy

Confocal fluorescence microscopy is a useful technique for making quantitative measurements of the fluorescence signal. The advantage of using confocal microscopy is the higher resolution that can be obtained (4096 x 4096 pixels). The fluorescence light that is emitted by the fluorophores and reaches the objective lens, is focused by another lens, aligned with the pinhole. This pinhole ensures that only the fluorescence signal from the focal plane is captured by the detector. This is the most important component of the confocal fluorescence microscopy because the fluorescence emission from above or below the focal point is blocked. The scanning mirrors are used to scan the whole sample and generate an image pixel by pixel.[51–53] To excite the fluorophore, multiple lasers can be used with a wavelength of 405, 488, 561 and 638 nm. With these different lasers the fluorescence signal of smaller and bigger coke species can be obtained. The fluorescence signal of the smaller coke species will be obtained with the 405 and the 488 nm laser. The 561 and 638 nm laser excited the fluorophores of the bigger coke species.[54]

Different detectors can be used to measure the fluorescence signal of a slice of the particle. With the DU4 detector the intensity of the fluorescence signal between a specific wavelength window can be obtained.[51] Another detector, that is called the Spectral Detector, a spectrum of the emission of the fluorescence signal can be obtained. Due to a laser shielding mechanism which eliminates the reflected laser light from the excitation source, all the lasers can be used during this measurement.[55] For this a multianode photomultiplier is used, with 32 detection channels of 10 nm to generate a separate image from each channel. The total bandwidth of the fluorescence emission depends on the grating, the number of channels, and therefore can be from 80 nm bandwidth to 320 nm bandwidth.

3. Experimental

3.1. Materials

- n-hexane (extra dry over molecular sieve 97%) from Acros Organics
- Ecat particles from Albemarle
- Fresh FCC catalyst from Albemarle

3.2. Preparation of coked FCC catalyst.

The Ecat samples with different amounts of coke species were obtained with a hexane cracking reaction. First the Ecat particles were calcined in air for 36h at 600 ˚C. For this reaction a hexane cracking set-up was used, shown in Figure 37 (Appendix). For this reaction 250 mg calcined FCC catalyst was placed in a fixed-bed reactor and heated to a temperature of 550 ˚C (10 ˚C/min) under a nitrogen flow of 5 ml/min. When the set temperature of 550 ˚C was reached, the nitrogen flow was switched through the bubbler with hexane for different times, 5, 15, 30 and 60 minutes. The temperature of the bubbler filled with hexane was 21˚C. The same reaction was performed with calcined fresh FCC catalyst (Fcat). The Fcat particles were calcined in air for 5h at 600 ˚C. For the cracking reaction the same amount of sample, and the same settings were used. So, four Ecat samples and four Fcat samples were obtained with different amounts of coke species.

3.2.1. Pulsed samples

The pulsed Ecat samples were prepared by Albemarle, 100 mg of Ecat was placed in a fixed bed reactor and after reaching the set temperature of 550 ˚C, multiple times 1 µl hexane was pulsed over the sample. Each sample had a different amount of hexane, 10 µl, 24 µl, 50 µl and 100 µl.

3.3. *Ex situ* measurements

The *ex situ* measurements are performed with the conventional Raman spectrometer (CCD) for the Raman spectrum and the time-gated Raman spectrometer (TGRS) for the fluorescence lifetime measurements. The Raman spectra are recorded with two different CCD's, the TGRS vs CCD and Ecat 15 and 30 minutes measurements are performed with the AvaRaman-532 HERO-EVO (Avantes) spectrometer equipped with a 25 µm slit, and a back-thinned TE cooled CCD Detector with 1024 × 58 pixels. The other Raman spectra are obtained with another CCD, AvaRaman-532 TEC (Avantes) spectrometer equipped with a 25 µm slit, and a back-thinned TE cooled CCD Detector with 1024 × 58 pixels. The fluorescence lifetime measurements were performed with the PicoRaman M1, from Timegate Instruments, equipped with 768 x 8 pixels.

The TGRS vs CCD measurements are recorded with an Olympus microscope (Olympus BX41M, 50x objective) connected to the Raman Microprobe (from Timegate instruments) was coupled to the CCD for the Raman spectrum and this coupling was switched to the time-gated Raman spectrometer for the fluorescence lifetime measurements. The excitation source was a 532 nm pulsed laser (150 kHz, 150 ps FWHM) with 10% laser power. The fluorescence lifetime measurements were recorded with a delay time between 4 and 10.22 ns with 312 steps of 0.02 ns. Each measurement was integrated for 105000 laser pulses. This is a total acquisition time of 218.4 s. From those spectra the four most optimal spectra are used, this is recorded in 2.8 s. The Raman spectra of the CCD were recorded with an integration time of 100 ms and 28 times averaged, with a total time of 2.8 s.

For the *ex situ* measurements an Olympus microscope (Olympus BX41M, 50x objective) connected to the Raman Microprobe (from Timegate instruments) was coupled to the Raman spectrometer and the time-gated Raman spectrometer, with a 50/50 beam splitter. The excitation source was a 532 nm pulsed laser (150 kHz, 150 ps FWHM) with 10% laser power. The fluorescence lifetime measurements were recorded with a delay time between 6 and 10.22 ns with 212 steps of 0.02 ns. The Raman spectra were recorded with an integration time of 100 ms and 200 times averaged.

3.4. *In situ* measurements

The *in situ* experiments were performed with a linkam stage (TMHS600), the set-up is shown in Figure 38 (Appendix). Around 1 mg of the calcined Ecat was placed on the cover glass in the linkamcell and one particle was selected with the microscope to be followed during the reaction. The sample was heated to 550 ˚C at a rate of 20 ˚C/min under a N_2 flow of 5 ml/min and the second step was stay at 550 ˚C for 2.5 h. The second step was used for the coking and the regeneration. The same temperature and the same flow were used during each *in situ* experiment. For the coking experiments a flow of 5 ml/min N_2 was used, this flow went through the bubbler filled with hexane. During the regeneration experiments a 2.5 ml/min N_2 flow and a 2.5 ml/min O_2 flow was used. The same setup and the same temperature program were used for the *in situ* experiments with the calcined Fcat.

3.5. Microscopy images

The images of the samples were recorded with a CS165CU/M 1.6 MP Color CMOS Camera (Zelux) which was integrated in the Microprobe. The images of the whole sample are obtained with 10x objective. The images of one single particle are obtained with a 50x objective.

3.6. Thermogravimetric analysis

The thermogravimetric analysis (TGA) experiments were performed with the Perkin Elmer 8000. The following temperature program was used, the temperature was heated to 800 ˚C with 10 ˚C/min under an oxygen flow of 45 ml/min. For each measurement around 5-10 mg of the sample was used.

3.7. Confocal fluorescence microscopy

For the confocal fluorescent microscopy (cfm) measurements, an inverted Nikon instruments A1 confocal fluorescence microscope was used. The measurements were performed with a 60x oil emersed objective. The instrument was coupled to a NIS elements advanced research software. The oil used for the measurements was immersion oil type F from Nikon. During the measurements four different laser were used: 405, 488, 561, 640 nm. The optimal measurement settings were chosen for each set of samples, so no oversaturation was seen.
To obtain a single slice and a spectrum of the fluorescence emission, two detectors were used, DU4 and Spectral Detector.

3.8. Data processing

To understand the fluorescence lifetime, the signal is fit with a linear combination of three different fluorescence components, illustrated in Figure 10. The first instantaneous component only contains convolution of a Gaussian function, due to the laser pulse, and the box function, due to the time gating (G x B). This describes both Raman scattering and

fluorescence signal that is as fast as the laser pulse. The second component is described by the convolution of a Gaussian function, a box function and with exponential decay (G x Bx E). This component has a fast decay, between 0.15 and 0.50 ns. The third component contains the same convolution as the second component but has a lifetime between 0.5 and 5.0 ns. Furter details about the fit procedure can be find in Vogel et al. 2023.[40]

To compare the *ex* situ measurements with each other, the Raman to Total Ratio (RTR (%)) can be used. This is calculated by using a fit procedure of the G band. For this procedure a 3th degree polynomial function is used to fit the background and a Lorentzian line shape is used to fit the G band.

The fit procedure of the Raman spectra of the *in situ* measurement started with a constructing of the normalized average spectrum between 20 and 40 minutes. These are spectra with a clear G band. For the fit procedure of the average spectrum a 3th degree polynomial function is used for the background and four Lorentzian line shapes are used to fit the D and G band. All the recorded spectra during the *in situ* measurement are fit to this polynomial and n times the contribution of 4 Lorentzian line shapes.

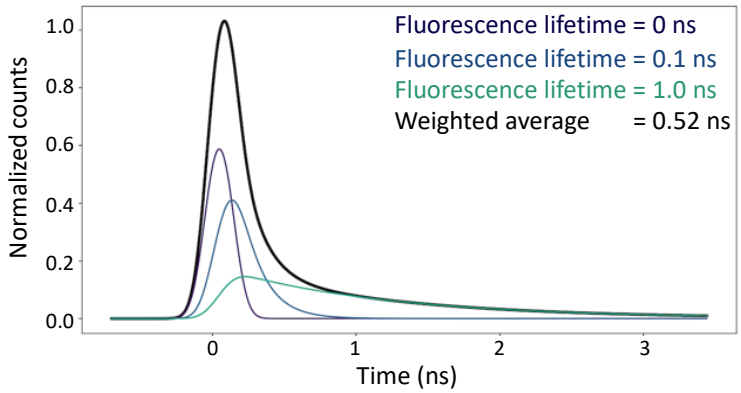

Figure 10: *example of the fit procedure for the fluorescence lifetime plot.*

4. Results and discussion

4.1. Microscopy pictures of all the samples

The microscopy images of all the prepared samples with different amounts of coke species are presented in Figure 11. Figure 11 A-D shows the images of the of the Ecat samples (continuous flow), these images show a heterogeneous distribution of the coke species over the particles. Figure 11A shows mostly light grey particles and Figure 11D has more darker grey colored particles. This means that the 60 minutes sample (Figure 11D) has more graphitic coke species and therefore more black colored catalyst particles. Figure 11 E-H shows the images of Ecat (pulsed) sample. These images have the same heterogeneous distribution of the coke species over the particles. This is because these samples are both Ecat particles, each particle has a different activity and therefore more or less coke species are formed at the catalyst particle. Figure 11 I-L shows the images of the Fcat samples, these images show a homogeneous distribution of the coke species over the catalyst particle. The amount of coke species increases with an increasing amount of hexane exposure, therefore Figure 11L is almost black. The homogeneous distribution of the coke species is due to the Fcat particles with particles with similar activity.

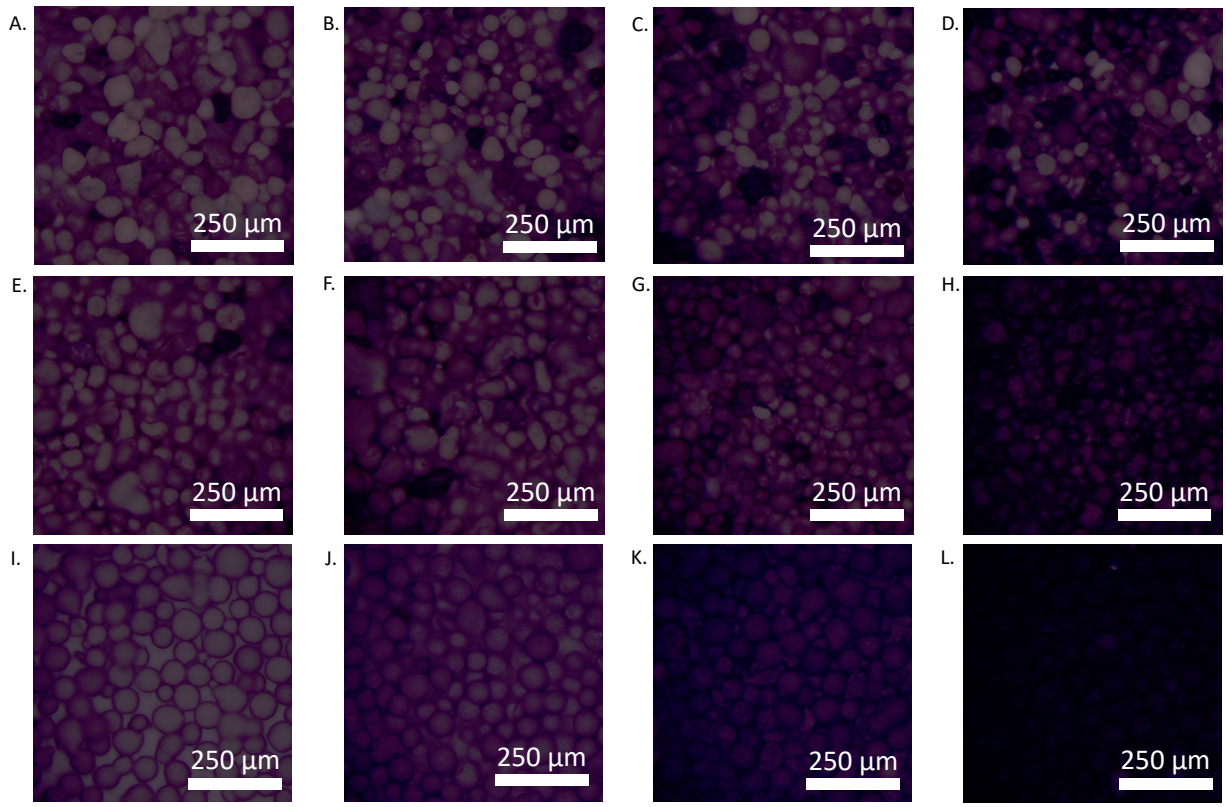

Figure 11: *Microscopy images of coked FCC catalyst particles. A-D Ecat samples (continuous flow), left to right: 5, 15, 30 and 60 minutes. E-H Ecat samples (pulsed), left to right: 10, 24, 50 and 100 µl. I-L Fcat samples, left to right 5, 15, 30 and 60 minutes.*

4.2. TGA

TGA measurements can be used to determine the amount of coke species on the catalyst. Therefore, all the different Ecat and Fcat samples are measured with TGA. The raw data of all the measurements is rather noisy and doesn't show horizontal plateau to use as a starting weight and end weight. Therefore, for each measurement, the average weight between 400-425 ˚C is used as starting weight and the range between 650-775 ˚C is used as final weight. To use a starting weight between 400 and 425 ˚C, the possible 'soft' coke is not taken into account and only the 'hard' coke is used to determine the amount of coke species.[20,56]

Figure 12A shows the raw data of the TGA measurements of the Ecat samples (continuous flow). The 5- and 15-minutes samples shows the lowest weight loss (%), 0.383% ± 0.013% and 0.424% ± 0.014% (Figure 12B). The 30 minutes sample has a weight loss of 0.519% ± 0.015%, and the 60 minutes sample has a weight loss of 0.659% ± 0.012% (Figure 12B). To determine if the weight loss is due to burning off the coke species or other organic components in the catalyst particles, calcined Ecat and Ecat are also measured. The Ecat sample has a weight loss of 0.249% ± 0.012% and the calcined Ecat has a weight loss of 0.236% ± 0.014%, the raw data is shown in Figure 39 (Appendix). The weight loss of the Ecat and calcined Ecat can be due to other organic components in the catalyst particle. This means that the amount of coke species is not equal to the weight loss (%).

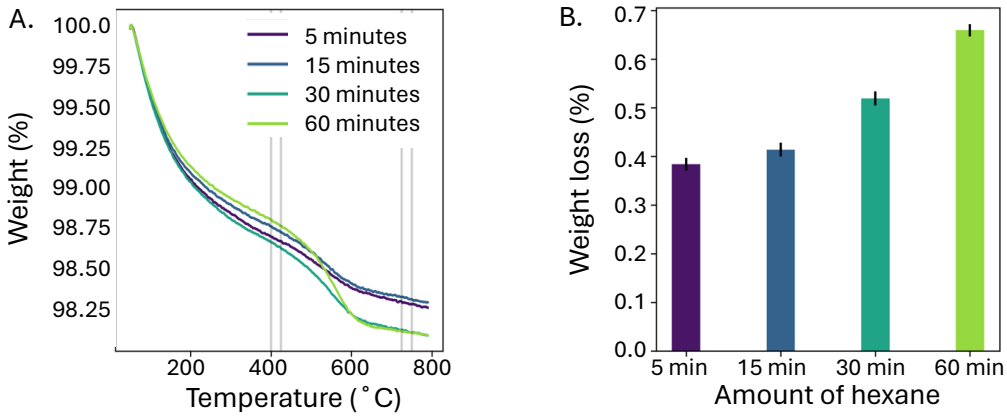

Figure 12: *A. Raw data of the TGA measurement of the Ecat samples (continuous flow), 5, 15, 30 and 60 minutes. B. Calculated amount of weight loss (%) with absolute uncertainty of the Ecat samples (continuous flow), 5, 15, 30 and 60 minutes.*

The pulsed Ecat samples shows a higher amount of weight loss compared to the samples with a continuous hexane flow, raw data is shown in Figure 13A. In this set of samples, the 10 and 24 µl also show the lowest weight loss (%), 0.498% ± 0.019% and 0.593% ± 0.021% (Figure 13B). The 50 µl sample has not a big increase of the weight loss compared to the 24 µl sample, 0.631% ± 0.020%. The 100 µl sample show the highest amount of weight loss, 1.234% ± 0.023%. This results in the same trend as the samples with continuous hexane flow, a higher amount of hexane results in a higher amount of weight loss. The pulsed experiments are performed with the same calcined Ecat as the continuous flow experiments. Therefore, the amount of coke species on the samples is lower than the amount of weight loss (%). Due to the noisy raw data of both Ecat samples it is not possible to plot the derivative of the weight loss (mg/K). The measurement can be improved by using more sample during the measurement so there is a higher weight loss (%).

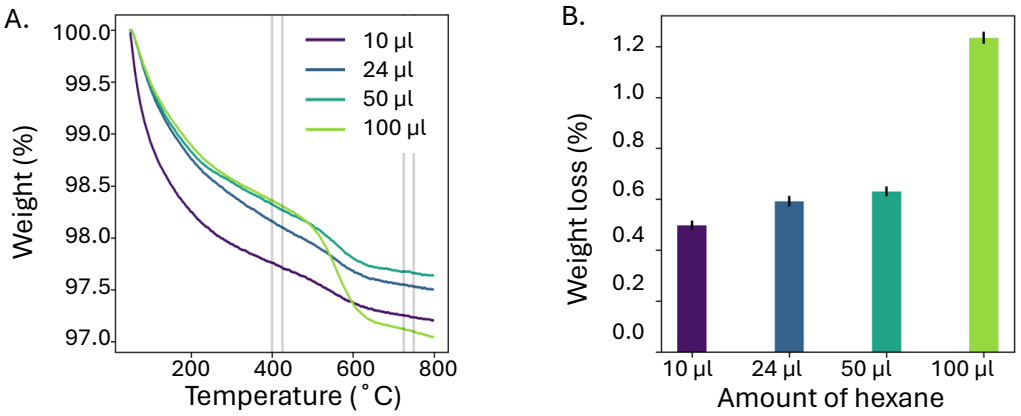

Figure 13: *A. Raw data of the TGA measurement of the Ecat samples (pulsed), 10, 24, 50 and 100 µl. B. Calculated amount of weight loss (%) with absolute uncertainty of the Ecat samples (pulsed), 10, 24, 50 and 100 µl.*

The last set of samples is the Fcat, raw data is shown in Figure 14A. The weight loss (%) of the 5- and 15-minutes sample are quite similar, 1.334% ± 0.063% and 1.482% ± 0.063% (Figure 14B). The 30 minutes sample shows a weight loss of 2.050% ± 0.064% and the 60 minutes sample shows a weight loss of 6.257% ± 0.053% (Figure 14B). There is a big difference between the weight loss of the 30 minutes sample and the 60 minutes sample. This is a different trend compared to the other 2 set of samples. But this can be due to a different reaction because it is fresh catalyst instead of Ecat. The calcined Fcat is also measured, raw data in Figure 39 (Appendix), the results show a weight loss of 1.197%. This weight is only because of water, the graph doesn't show a drop as the other samples do. Figure 14C shows the derivative of the weight loss (mg/K), this graph shows a large peak of the 60 minutes sample. However, the 5 minutes sample have a small peak around 300 ˚C, this peak is due to the 'soft' coke species. The other samples don't show a peak of the 'soft' coke species.

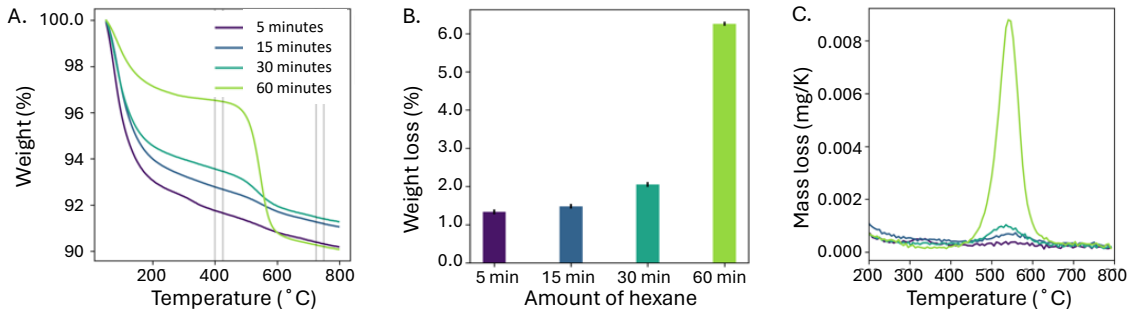

Figure 14: *A. Raw data of the TGA measurement of the Fcat samples, 5, 15, 30 and 60 minutes. B. Calculated amount of weight loss (%) with absolute uncertainty of the Fcat samples, 5, 15, 30 and 60 minutes. C. Derivative of the weight loss (mg/K) of the Fcat samples, 5, 15, 30 and 60 minutes.*

4.3. CFM

All the samples are measured with the confocal fluorescence microscope. Two different detectors are used for these measurements, with the DU4 a slice and a z-stack of slices (3D scan) are obtained. The spectral detector is used to obtain a spectrum of the emission of the fluorescence signal. From every sample three particles are measured with both detectors. The particles are probed with a 405, 488, 561 and 638 nm laser. All particles are measured with the same laser power and the HV is optimized for each set of samples. With these two detectors the fluorescence intensity of the coke species at different wavelengths can be determined. This can give an indication of different types of coke species.

In Figure 15 the z-stack of the 3D scan of one particle of the 60 minutes Ecat sample is shown, which are obtained with the DU4 detector. The coke species that are excited with the 405 and 488 nm lasers are the smallest coke species, monomers (Figure 15 A/B). The coke species that are excited with the 561 and 638 nm lasers are conjugated coke species, linear poly aromatic carbocations (Figure 15 C/D).[57–59] Figure 15 shows that the fluorescence signal of the 405 and the 488 nm lasers are less intense compared to the 561 and 638 nm lasers. This is as expected, the 60 minutes sample has less smaller cokes species and more larger coke species, due to an increasing exposure time of hexane. Therefore, the fluorescence intensity is higher for the 561 and 638 nm laser. However, with the DU4 detector it is difficult to compare the different samples with each other.

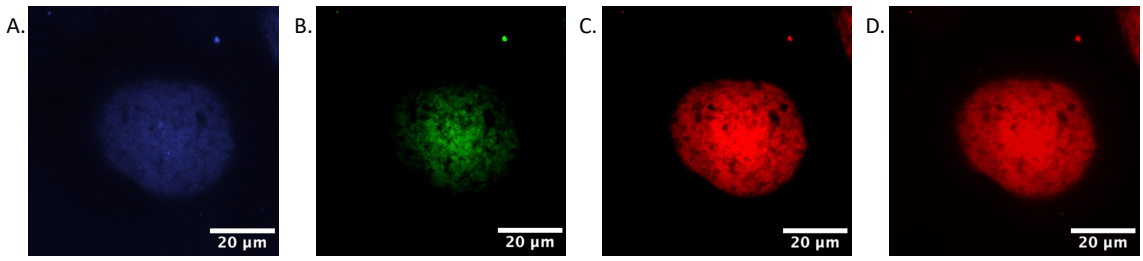

Figure 15: *z-stack of obtained slices of one particle, 60 minutes Ecat sample.*

To compare the different samples the spectral detector mode is used to obtain the fluorescence spectrum. The fluorescence spectrum is recorded in a wavelength window between 430 and 750 nm. Therefore, the spectrum will show the fluorescence emission of the blue, green, yellow and red part of the spectral range. In the Figure 16, 17 and 18 the graphs of the average of three particles of each sample are shown. To compare the four different samples, the graphs are normalized at two points, 470 nm (Figure A) and 670 nm (Figure B).

4.3.1. Ecat continuous flow

The normalized results at 470 nm (Figure 16A) illustrates a similar graph for the four samples in the blue and green part of the spectral range. In the yellow and red part of the spectrum there are some differences between the four samples; the 5- and 15-minutes samples show the lowest intensity, and the 30- and 60-minutes samples show a higher intensity of the fluorescence signal. This means that the 60 minutes sample has the highest fluorescence intensity, this can be due to relatively more larger fluorescent coke species.[57,59] The graph normalized at 670 nm (Figure 16B) shows that the red part of the spectral range has almost the same result for all the samples. In this graph the blue and green part of the spectral range

shows differences between the four samples. In both parts the 30- and 60-minutes samples shows the lowest fluorescence intensity compared to the 5- and 15-minutes samples. The 5 minutes sample has the highest fluorescence intensity in the blue and green part of the spectral range, this can be due to relative more smaller coke species. The dips between the blue, green, yellow and red parts of the spectral range come from the filters in the detector which eliminates the reflected laser light of the excitation source.

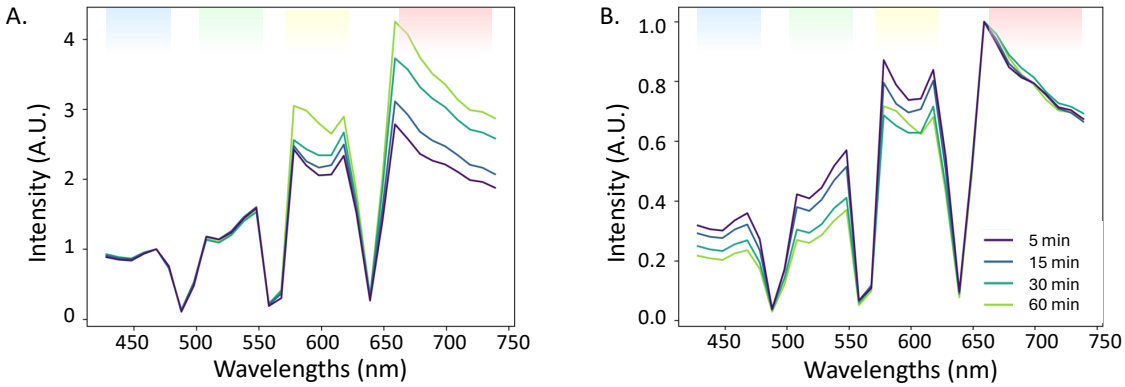

Figure 16: *Fluorescence intensity spectrum of the confocal fluorescence microscopy spectral detector of Ecat samples (continuous flow). A. Normalized at 470 nm. B. Normalized at 670 nm.*

4.3.2. Ecat pulsed

Figure 17A illustrates that the blue and green part of the spectrum the four samples shows almost the same fluorescence intensity if the graph is normalized at 470 nm. The yellow and red part of the spectral range shows a difference between the four samples; in this part the 10 and 24 µl samples show the highest intensity and the 100 µl sample has the lowest fluorescence intensity. This trend is different compared to the Ecat (continuous flow) sample. This can be due to difference in grey value of the sample, the pulsed Ecat samples have a higher grey value which means more graphitization of the coke species and the graphitic coke species are not fluorescence anymore.[60] This can result in a lower fluorescence intensity for the 50 and 100 µl sample.

Figure 17B shows almost the same intensities for the four samples at the red part of the spectral range. The blue and green part of the spectral range shows differences. The 50 and 100 µl samples shows the highest fluorescence signal and the 10 and 24 µl have the same fluorescence intensity. Also, this trend is different compared to the Ecat (continuous flow), the expectation was that the 10 and 24 µl samples has the highest intensity in the blue and green part. This is not the case for this sample; however, these results are based on only three particles, it can be that this is not enough to see the trend of the fluorescence intensity of the samples. Compared to the TGR measurements, 75 particles were measured to see a trend in the samples. This was not possible for the CFM measurements because only 4 particles can be measured on one day.

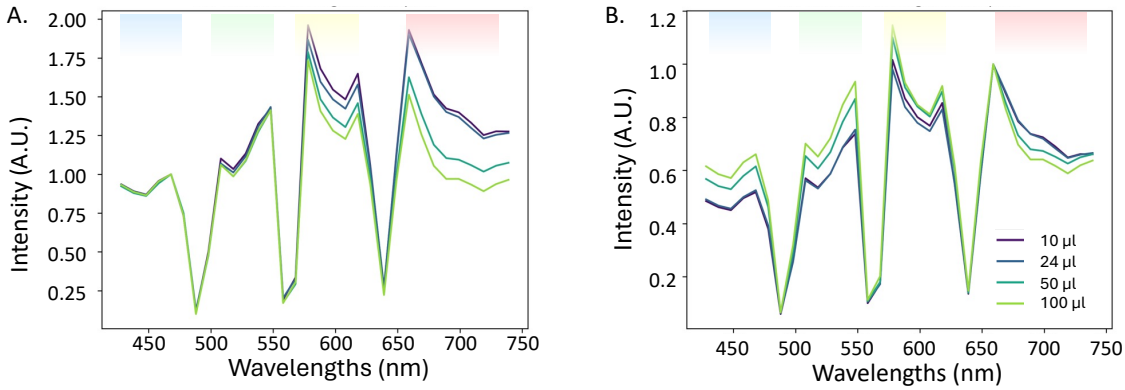

Figure 17: *Fluorescence intensity spectrum of the confocal fluorescence microscopy spectral detector of Ecat samples (pulsed). A. Normalized at 470 nm. B. Normalized at 670 nm.*

4.3.3. Fresh catalyst

Figure 18A illustrates that the in blue part of the spectral range the four samples almost have the same fluorescence intensity. The yellow and red part of the spectral range shows a big difference in intensity between the four samples. The 5- and 15-minutes samples shows the highest fluorescence intensity, and the 60 minutes samples shows the lowest intensity. This is a different trend compared to the Ecat (continuous flow) but this can be due to the really high grey value of these samples. The 30- and 60-minutes samples are almost black, so they have a high amount of graphitic coke species and thus a lower fluorescence signal. The graph normalized between at 670 nm (Figure 18B) shows in the red part of the spectral range not all the samples have the same fluorescence intensity, but they are a bit similar. The blue and green parts show differences between the samples, the 5- and 15-minutes samples has the lowest intensity, and the 60 minutes has the highest fluorescence intensity. This is the same trend as the Ecat (pulsed), this means that the 30- and 60-minutes samples has relatively the highest amount of small fluorescence coke species.

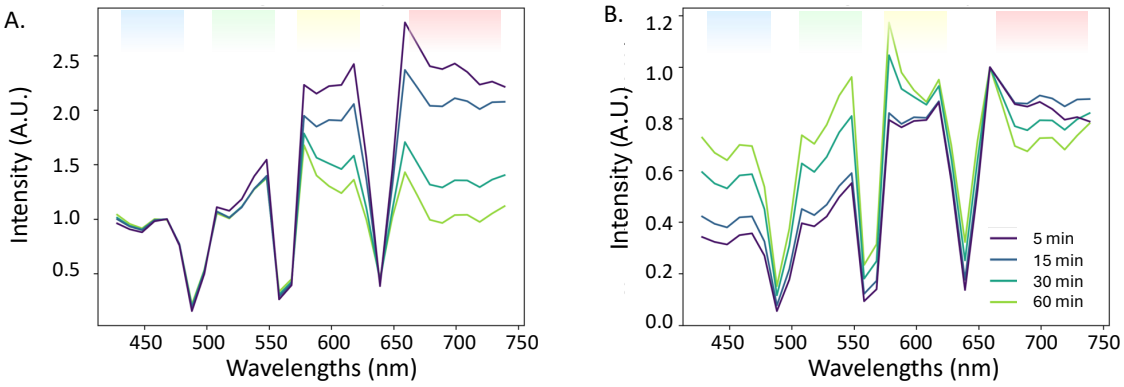

Figure 18: *Fluorescence intensity spectrum of the confocal fluorescence microscopy spectral detector of Fcat samples. A. Normalized at 470 nm. B. Normalized at 670 nm.*

4.4. Raman spectroscopy and fluorescence lifetime measurements

4.4.1. Time-gated Raman spectrometer vs. conventional Raman spectrometer

To determine the differences between the Raman spectrum recorded with the time-gated Raman spectrometer (TGRS) and the conventional Raman spectrometer (CCD), 20 spots of the 60 minutes sample are measured with both spectrometers. The spectrum recorded with the TGRS is the average of the four most optimal spectra from the TGRS data set, this spectrum is compared to the spectrum recorded with the CCD. Figure 19A shows the Raman spectrum recorded with the TGRS and the CCD. This graph shows that in both spectra there is a small G band around 1600 cm^{-1}, this is due to the vibration of the graphitic coke species. The D band, vibration of the edges of the coke species, is not visible in both spectra due to background noise.[23,61] The spectrum recorded with the TGRS has a lower background compared to the spectrum obtained with the CCD. This is due to the detector of the TGRS that is only activated during a specific portion of time, which lowers the random background noise of the spectrum. Due to the lower background of this spectrum the G band is more prominent with respect to the background. However, all the D and G bands in the spectra recorded with the TGRS, are also visible in the spectra recorded with the CCD. One big difference between both spectra is the signal-to-noise ratio (SNR). The spectrum recorded with the TGRS is noisier compared to the spectrum recorded with the CCD. This means that the SNR of the Raman spectrum recorded with the CCD is much higher, this is due to a more sensitive detector compared to the detector of the TGRS. So, the conclusion is that the Raman spectrum recorded with the CCD has a higher quality compared to the spectrum obtained with the TGRS. However, with a TGRS measurement the heatmap shown in Figure 19B can also be obtained. This a heatmap of the Raman spectrum and shows the G band in the spectrum. Scanning over the signal with a specific time-gate will result in a time trace of the fluorescence signal. This fluorescence lifetime plot can give information about the nature of the fluorescence signal.

All the upcoming samples are measured with the TGRS, for the fluorescence lifetime measurement and the CCD, for the Raman spectrum. These two detectors can be used at the same time, by using a 50/50 splitter.

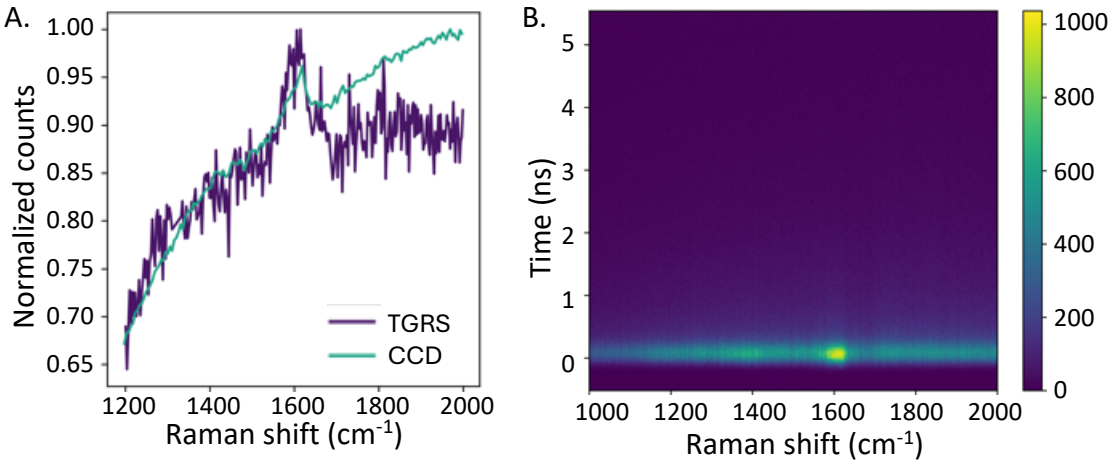

Figure 19: *A. Raman spectrum recorded with time-gated Raman spectrometer compared to the Raman spectrum recorded with the conventional Raman spectrometer. B. Heatmap obtained with the time-gated Raman spectrometer.*

4.4.2. *Ex situ* experiments

To investigate in the nature of the carbon deposits on the coked FCC samples, fluorescence lifetime measurements are combined with Raman spectroscopy. From each Ecat/Fcat samples 75 particles are measured. The fluorescence lifetime measurements are performed with the time-gated Raman spectrometer and the Raman spectrum is recorded with the conventional Raman spectrometer. The measurements are performed with the same measurement settings, for all the samples. For each fluorescence signal a time trace fit is used determine the contributions of three different components, explained in chapter 3.8. With the results of the time trace fit, the weighted average of each fluorescence lifetime measurement is calculated.

4.4.2.1. Ecat continuous flow

All the 75 measured particles show a variety of different Raman spectra and fluorescence lifetime plots. This is due to the different activities of the catalyst particles. To illustrate the need of a Raman spectrum and a fluorescence lifetime plot of the same particle, four different particles of the 60 minutes sample are shown in Figure 20. Each particle has a different Raman spectrum and a different fluorescence lifetime plot, shown in Figure 20 E-F.

Particle one (Figure 20A) is a light grey particle and the Raman spectrum (Figure 20E) shows no D/G band. Figure 20F shows a fluorescence lifetime plot with a long decay. Comparing this particle with particle 4 (Figure 20D) a dark grey particle. This particle has a D and G band in the Raman spectrum and a fluorescence lifetime with a short decay. For these two particles the trend is that a darker grey particle has a shorter fluorescence lifetime and D and G bands in the Raman spectrum. However, particles two and three give different results. Particle two and three (Figure 20B and C), one grey particle and the other very light grey. The Raman spectrum of particle two has a small G band in the Raman spectrum, however particle three shows a more intense G band and a D band. Nevertheless, the fluorescence lifetime plots of the two particles are the same. This means that with only the Raman spectrum or only the fluorescence lifetime plot not the right conclusion can be formed about the particle. However, the results of the Raman spectrum and the fluorescence lifetime plot are complementary to each other. These four particles do not have all the same trends, such as a higher grey value of the particle results in a shorter decay of the fluorescence lifetime and a higher RTR value of the G band. To find trends in a sample the average Raman spectrum and the average lifetime plot can be used. With these spectra also the samples can be compared to each other.

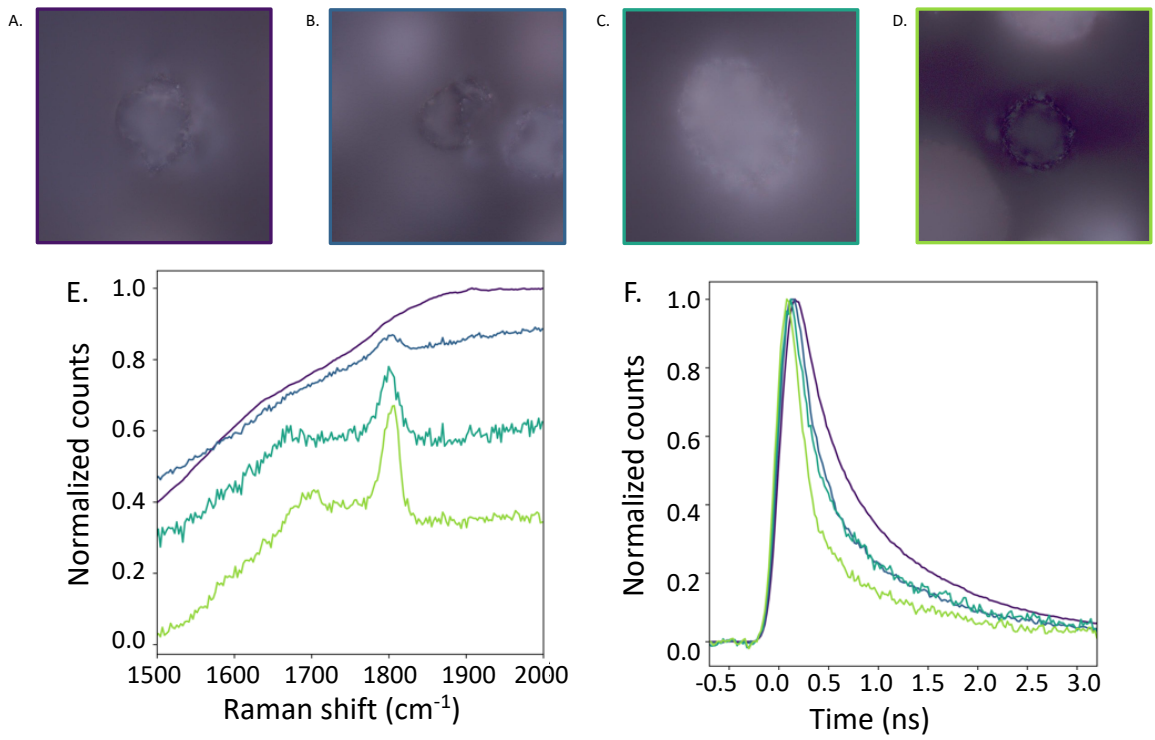

Figure 20: *A-D microscopy images of four different particles of the 60 minutes sample (Ecat continuous flow). E. Raman spectra of the four particles. F. Fluorescence lifetime plot of the four particles*

To compare the four different samples, the average fluorescence lifetime plot of the four samples is shown in Figure 21A/B. This graph shows that the average fluorescence lifetime of the 15 minutes sample increases compared to the 5 minutes sample. This means that the fluorescence signal of the 15 minutes sample has a slower decay compared to the 5 minutes sample. The fluorescence lifetime plotted at log scale (Figure 21B) shows a better difference between the 5- and 15-minutes samples. The fluorescence lifetime of the 30 minutes sample has a faster decay compared to the 5- and 15-minutes sample and the 60 minutes sample has the fastest decay. So, the fluorescence lifetime will first increase with an increasing time of hexane, followed by a decrease. The average Raman spectrum (Figure 21C) can also be used to compare the different samples. In the average spectrum there are no D/G bands in the spectrum of the 5-, 15- and 30-minutes sample. The spectra of the 15- and 30-minutes sample are almost the same. In the spectrum of the 5 minutes sample, there is a broad peak between 1400 and 1600 cm^{-1}, due to the high fluorescence signal of the coke species.[23] In the average spectrum of the 60 minutes sample, there is a small G band. This means that an increasing amount of hexane leads to a more intense D and G bands in the Raman spectrum.

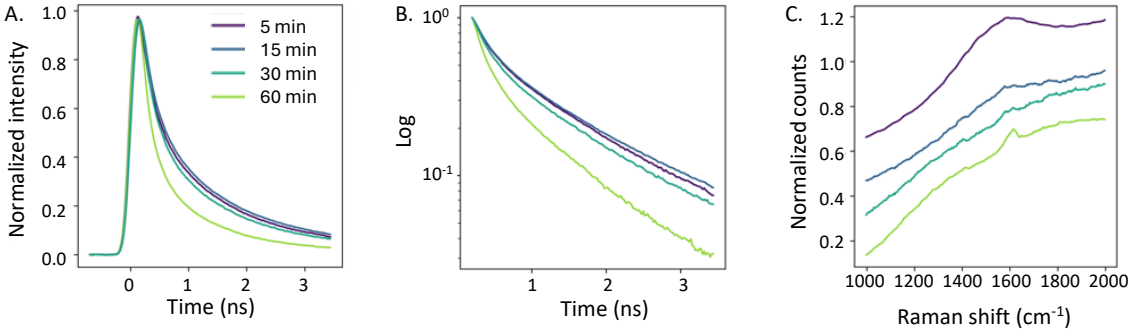

Figure 21: *A. Average fluorescence lifetime plot of the four Ecat samples (continuous flow). B. Log scale of graph A. C. Average Raman spectrum of the four Ecat samples (continuous flow).*

Figure 22A-D shows the distribution of the weighted averages of all the samples. These plots show that there is a small shift to zero comparing the 5- and 60-minutes sample. Figure 22E shows the average weighted average of each sample including the error bar. This plot shows the same trend as the average fluorescence lifetime plot, the sample weighted average of the 15 minutes sample is increased compared to the 5 minutes samples. The 30 and 60 minutes show a decrease of the sample weighted average, compared to the 15 minutes sample. This means that the sample weighted average shows the same trend as the average fluorescence lifetime plots.

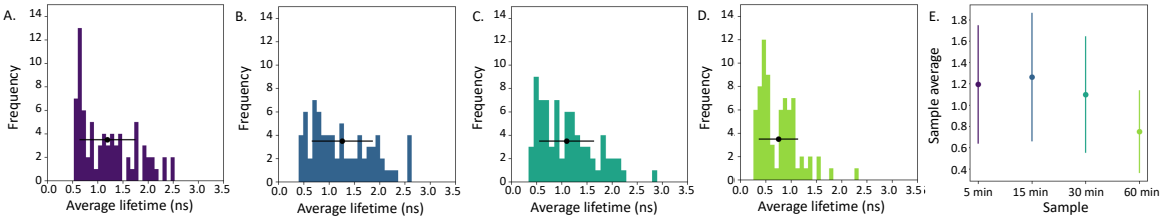

Figure 22: *A. Distribution of the weighted average and error bar of 5 minutes samples. B. Distribution of the weighted average and error bar of the 15 minutes samples. C. Distribution of the weighted average and error bar of the 30 minutes samples. D. Distribution of the weighted average and error bar of the 60 minutes samples. E. Average weighted average of the 5, 15, 30 and 60 minutes Ecat samples.*

Correlation plots can be used to see if there is a correlation between the weighted average fluorescence lifetime and the RTR (%). In Figure 23A the weighted average of the fluorescence lifetime and the RTR are plotted for the 15, 30 and 60 minutes the correlation is slightly negative, -0.21 and -0.36. This means that there is a no correlation between the weighted average and the RTR value. The correlation between the three components of the fit procedure and the RTR (%) are shown in Figure 23 B-D. The 15-, 30- and 60-minutes sample show that there is a weak to moderate correlation between the contribution of component 1 and RTR (%) (Figure 23B), 0.52, 0.46 and 0.52. The correlation between the contribution of component 2 and RTR (%) is for the 15-, 30- and 60-minutes sample is around zero for all three samples (Figure 23C). This means there is no correlation. The correlation between the contribution of component three and RTR varies between -0.24 and -0.44 (Figure 23D). This means that there is a weak anti-correlation and the RTR will decrease with an increasing contribution of component three.

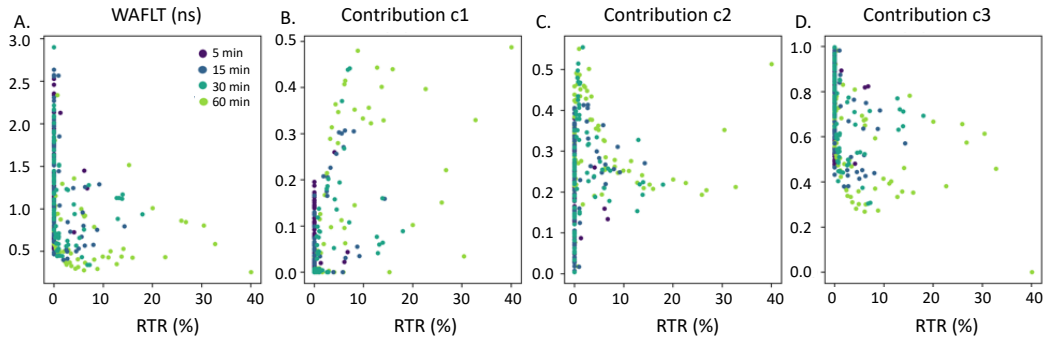

Figure 23: *A. Correlation plot of the weighted average vs RTR (%). B. Correlation plot of the contribution of component 1 vs RTR (%). C. Correlation plot of the contribution of component 2 vs RTR (%). D. Correlation plot of the contribution of component 3 vs RTR (%).*

4.4.2.2. Ecat pulsed

As shown for the Ecat samples with continuous flow, the fluorescence lifetime plot, the Raman spectrum, and the grey value of the particle, do not always show the same trends, higher amount of coke species results in a higher RTR value and a lower fluorescence lifetime. Figure 24 shows the microscopy images of four different particles of the 50 µl sample, the fluorescence lifetime plot, and the Raman spectrum. The fluorescence lifetime plots (Figure 24 F) shows that particle one and two have almost the same fluorescence lifetime and particle 3 and four as well. But the Raman spectrum (Figure 24E) of the two particles is not the same. Particle one doesn't show D/G bands and particle 2 show a G band and a very broad D band. The fluorescence lifetime is almost the same, but the grey value of the particle is not the same. Particle two has a higher grey value, therefore the G band can appear in the Raman spectrum. Particle three and four both have a higher grey value, compared to the other two particles but shows almost the same fluorescence lifetime. Particle four shows bigger D/G bands compared to particle 3. This can be due to bigger coke species but both particles have graphitization of the coke species and therefore the fluorescence lifetime can be almost the same. This shows the same trend as the four particles with the continuous flow, only the Raman spectrum or the fluorescence lifetime, is not giving all the information about the coke species on the catalyst particle but giving complementary information about the coke species.

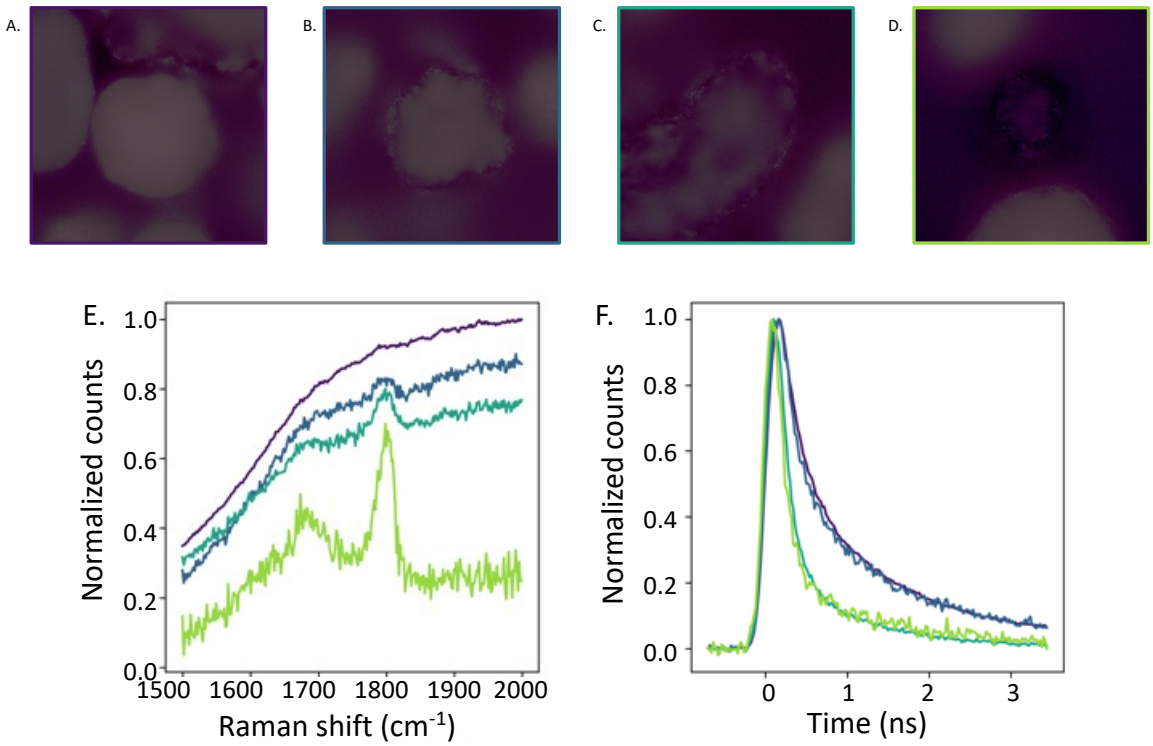

***Figure 24**: A-D microscopy images of four different particles of the 50 µl sample (Ecat pulsed). E. Raman spectra of the four particles. F. Fluorescence lifetime plot of the four particles.*

To compare the four pulsed samples, the average fluorescence lifetime (Figure 25 A/B) and the average Raman spectrum (Figure 25C) can be used. The fluorescence lifetime of the 10 and 24 µl sample are almost the same. There is a small difference at the tail of the graph, here the fluorescence signal of the second sample, 24 µl, has a longer lifetime compared to the 10 µl sample. In Figure 25B the fluorescence lifetime is plotted at log scale, the zoomed part of the graph shows the small difference between the fluorescence lifetime of the 10 and 24 µl sample. This is the same trend as the Ecat samples with continuous flow, but in that set of samples it is clearer. This can be due to the difference in the amount of hexane and the particle (microscopy images, Figure 11) looks different, greyer colored so the first and second sample already have more coke species. The average fluorescence lifetime of the 50 µl sample is shorter compared to the 10 µl sample. The 100 µl sample has the shortest fluorescence lifetime compared to the other samples. This is the same trend as the set of samples with the continuous flow. This is also in line with the literature, more graphitization results in less fluorescence signal, so the fluorescence lifetime will be more like Raman signal. In the average spectrum of the 10 µl sample, there is a small broad peak in the spectrum, this is due to the intense fluorescence signal of smaller coke species. The second sample, 24 µl, shows a small G band in the Raman spectrum. The 50 µl sample has a G band and a small D band. The 100 µl sample has a big G band and a D band in the Raman spectrum. This is the same trend as the set of samples with the continuous flow. This is also in line with the literature, more graphitization results in less fluorescence signal, so the fluorescence lifetime will be more like Raman signal.

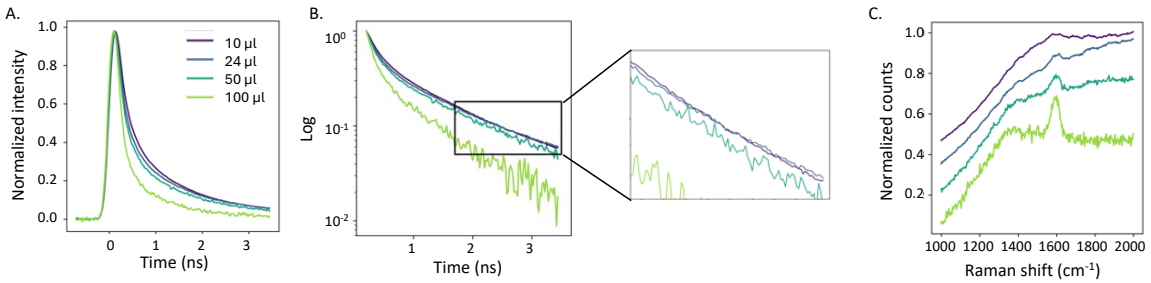

Figure 25: *A. Average fluorescence lifetime plot of the 10, 24, 50 and 100 µl Ecat samples. B. Log scale of graph A. with a zoom of a part of the graph. C. Average Raman spectrum of the 10, 24, 50 and 100 µl Ecat samples.*

The histograms, shown in Figure 26 A-D, can also be used to show the distribution of the weighted average of the fluorescence lifetime of all the spots of the sample. The histogram shows the same trend as the fluorescence lifetime plots. The average weighted averages of the samples are, 1.071 ± 0.479 ns, 1.100 ± 0.555 ns, 0.997 ± 0.446 ns, 0.572 ± 0.228 ns. Because of the small differences between the 5- and 15-minutes samples, Figure 26E shows the sample weighted average. This plot illustrated the same trend as the average fluorescence lifetime plot.

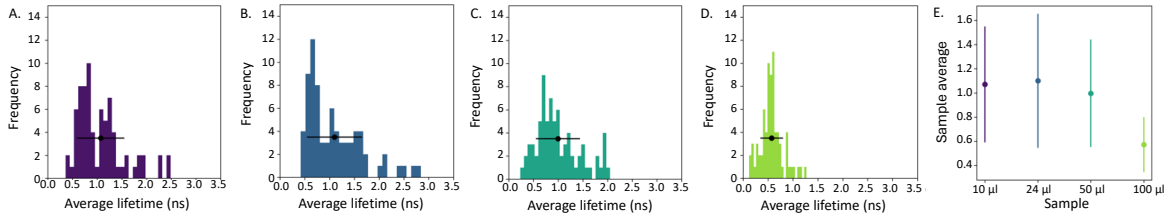

Figure 26: *A. Distribution of the weighted average and error bar of 10 µl samples. B. Distribution of the weighted average and error bar of the 24 µl samples. C. Distribution of the weighted average and error bar of the 50 µl samples. D. Distribution of the weighted average and error bar of the 100 µl samples. E. Average weighted average of 10, 24, 50 and 100 µl Ecat samples.*

The correlation plots can be used to see if there is a correlation between the weighted average fluorescence lifetime and the RTR (%). Figure 27A shows that the correlation between those two components is negative for all the four samples. This means that the there is an anti-correlation between the weighted average of the fluorescence lifetime and the RTR (%). Figure 27B shows the correlation of the contribution of component 1 and the RTR (%). The correlation for the 5, 15, 30 and 60 minutes is, 0.67, 0.70, 0.58 and 0.76. This means that there is a moderate correlation between the contribution of component one and the RTR (%). Figure 27C shows the correlation between the contribution of component 2 and the RTR (%), for all the samples this is slightly negative. So, this means that there is no correlation between the contribution of component 2 and RTR (%). Figure 27D shows the correlation between the contribution of component 3 and the RTR. This plot shows a negative correlation between -0.5 – -0.7, this means that there is a moderate negative correlation between the contribution of component 3 and the RTR. The RTR value will decrease with an increasing contribution of component 3.

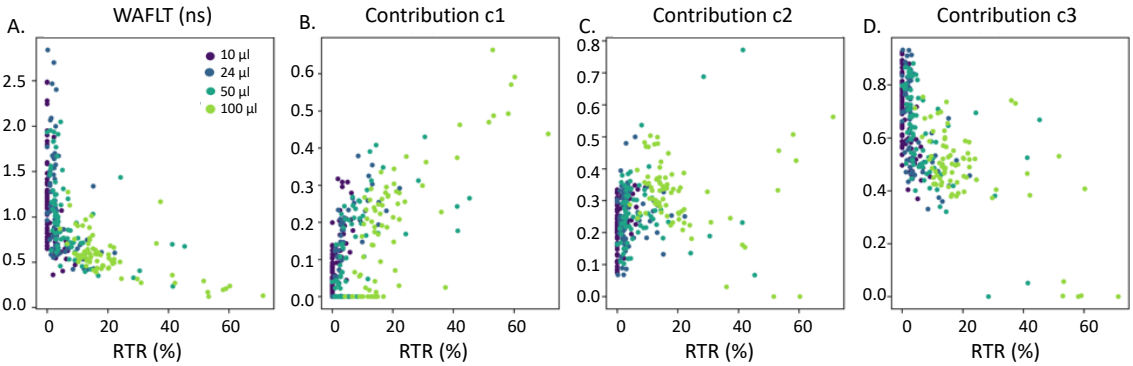

Figure 27: *Correlation plot of the weighted average vs RTR (%). B. Correlation plot of the contribution of component 1 vs RTR (%). C. Correlation plot of the contribution of component 2 vs RTR (%). D. Correlation plot of the contribution of component 3 vs RTR (%).*

4.4.2.3. Fresh catalyst

To compare the four different Fcat samples, the average Raman spectrum, and the average fluorescence lifetime of all the samples can be used. In Figure 28 A-B the average fluorescence lifetime of the four different Fcat samples. The 5 minutes sample is around 0.894 ns and the fluorescence lifetime of the 15 minutes sample is 0.583 ns. However, the fluorescence lifetime of the 30 minutes sample is longer compared to the 5- and 15-minutes sample, 1.055 ns. The fluorescence lifetime of the 60 minutes sample is 1.136 ns, this is longest fluorescence lifetime of this sample. This means that the average lifetime of the Fcat samples show first a decrease and after that an increase of the fluorescence lifetime with an increasing exposure time of hexane. This is not the same trend compared to the fluorescence lifetime of the Ecat samples. Figure 28C shows the average Raman spectrum of the four Fcat samples. In the average Raman spectrum of the 5- and 15-minutes samples, there is no D/G band in the spectrum. This was expected because there were no Raman spectra with D/G bands of all the 75 measured spectra. In the spectrum of the 30 minutes sample there is a small G band and a very small and broad D band. The average spectrum of the 60 minutes sample shows the most intense D and G bands of this set of samples. This means that an increasing exposure of hexane results in an increasing amount of graphitic coke species. The average Raman spectrum shows the same trend as the average Raman spectrum of the Ecat samples.

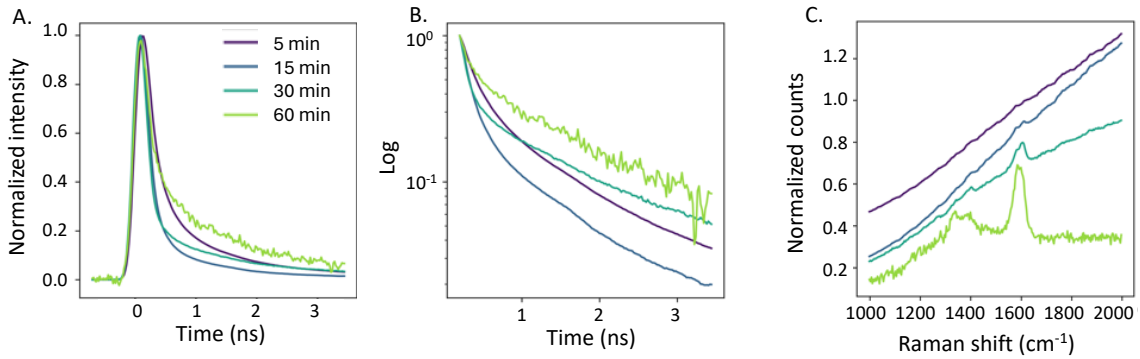

Figure 28: *Average fluorescence lifetime plot of the four Fcat samples. B. Log scale of graph A. C. Average Raman spectrum of the four Fcat samples.*

The histograms can also be used to compare the four different samples, shown in Figure 29A-D. The histograms show the distribution of the weighted averages of the four different samples. These plots show that the distribution of the weighted average is broadened comparing the 5 minutes sample with the 60 minutes sample. Figure 29E illustrates the sample weighted average of all the samples. The 15 minutes sample shows a decrease compared to the 5 minutes sample and the 30- and 60-minutes samples show an increase. This means that this plot shows the same trend as the average fluorescence lifetime plot.

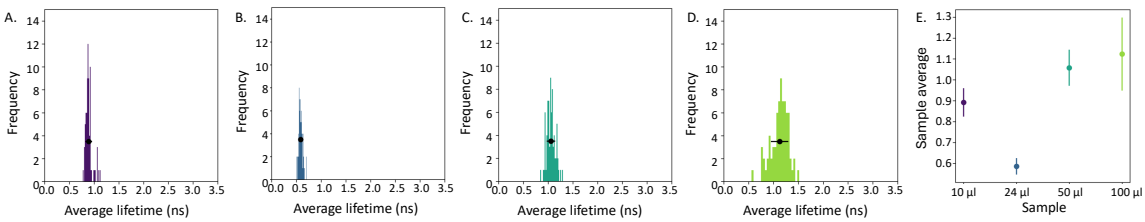

Figure 29: *A. Distribution of the weighted average and error bar of 5 minutes Fcat sample. B. Distribution of the weighted average and error bar of the 15 minutes Fcat sample. C. Distribution of the weighted average and error bar of the 30 minutes Fcat sample. D. Distribution of the weighted average and error bar of the 60 minutes Fcat sample. E. Average weighted average of 5, 15, 30 and 60 minutes Fcat samples.*

As mentioned before, correlation plots can be used for the correlation between the weighted average fluorescence lifetime and the RTR (%). Figure 30A shows the correlation plots of the weighted average of the fluorescence and the contribution of the three different components and the RTR value. The 5 minutes sample has a moderate correlation between the weighted average and the RTR of 0.58. The 15- and 30-minutes samples show no correlation between the weighted average and the RTR (%). The 60 minutes sample has a correlation of -0.74. This means that there is a strong anti-correlation between the weighted average and the RTR. The RTR value will decrease with an increasing weighted average. This is not the same trend as the Ecat samples, but the histogram of the Fcat samples shows the same trend. Figure 30 D-E shows the correlation between the contribution of the three different components and the RTR (%). Figure 30B shows the contribution of component 1 and RTR (%), for the 5- and 15-minutes samples this is 0.56 and 0.57. This means that there is a moderate correlation. The 30 minutes samples have a correlation of 0.15, so there is no correlation. The 60 minutes sample have a correlation of 0.68. This means that there is a correlation between the contribution of component 1 and the RTR (%). Figure 30C shows the correlation between component two and the RTR (%), the 5- and 15-minutes sample have a moderate negative correlation. The 30- and 60-minutes sample have a weak negative correlation. Figure 30D shows the correlation between the contribution of component 3 and the RTR is for the 5-, 15- and 30-minutes sample around zero, so no correlation. However, the 60 minutes sample has a correlation of -0.81. This means that the RTR value will decrease with an increasing contribution of component 3. This trend is also visible in the histogram and the average fluorescence lifetime plot. The 60-minute sample has the highest average weighted average.

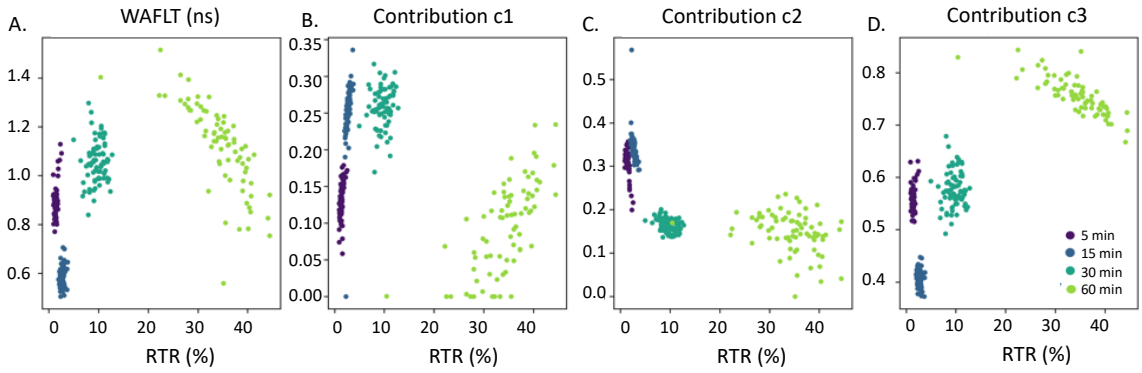

Figure 30: *Correlation plot of the weighted average vs RTR (%). B. Correlation plot of the contribution of component 1 vs RTR (%). C. Correlation plot of the contribution of component 2 vs RTR (%). D. Correlation plot of the contribution of component 3 vs RTR (%).*

4.4.3. *In situ* experiments

4.4.3.1. Ecat

To get more information about the formation of the coke species at the catalyst particle, *in situ* experiments are performed. The fluorescence lifetime measurements and the Raman spectrum of the particle are obtained using a 50/50 beam splitter and a linkam cell is used to reach the temperature of 550 ˚C. The *in situ* coking experiments are performed with the hexane bubbler and for the *in situ* regeneration a gas flow of 50/50 N_2/O_2 is used. The O_2 gas flow is used to burn off the coke species. During the *in situ* measurements the same particle is measured for 60 minutes. There are 5 coking and 4 regeneration reactions performed with five different calcined Ecat particles. During one regeneration reaction the time-gated Raman gave an error and there are no results obtained. Each catalyst particle is different and have a different activity, so the expectation is that each experiment has a different result.

The results of the *in situ* coking measurement are shown in Figure 31. Figure 31A shows a few fluorescent lifetime measurements, 0, 1, 15 and 25 minutes. The fluorescence lifetime plot of 1 minute, has a shorter decay compared to the 0 minutes measurement. The fluorescence lifetime plot of the 15- and 25-minutes show a decrease of the fluorescence lifetime. This means that a longer exposure time of hexane results in an increase followed by a decrease of the fluorescence lifetime. Figure 31B shows a heatmap of the whole *in situ* measurement, this heatmap illustrates the upcoming G band in the Raman spectrum, this is illustrated due to the color change around 1600 cm^{-1}. In the heatmap it is difficult to see at which time the G bands appears in the Raman spectrum. Therefore, in Figure 31C a few Raman spectra are shown, 0, 8, 10 and 20 minutes. This illustrates that the G band appears between 8-10 minutes in the Raman spectrum.

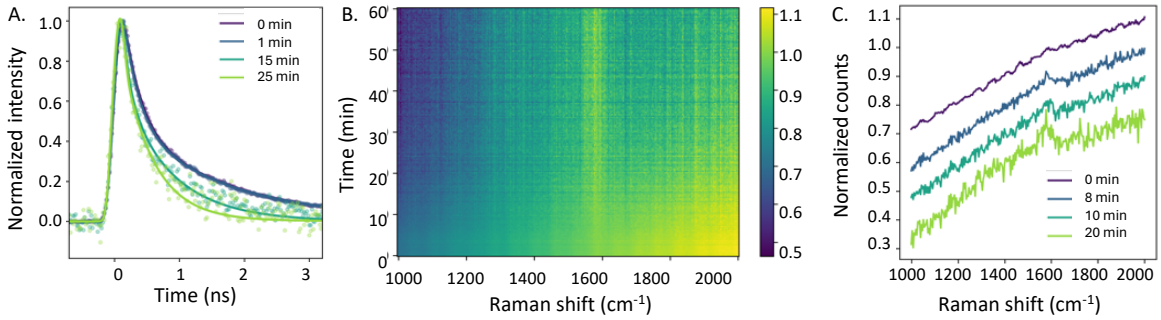

Figure 31: *Results of the in situ coking of Ecat. A. Fluorescence lifetime plot at 0, 1, 15 and 25 minutes. B. Heatmap of the Raman spectrum (0-60 minutes). C. Raman spectra at 0, 8, 10, 20 minutes.*

The fluorescence lifetime plot of the *in situ* experiments and the average fluorescence lifetime plot of the *ex* situ measurements show an increase followed by a decrease with an increasing exposure time of hexane. This means that if the small coke species start growing the fluorescence lifetime will increase. However, the fluorescence lifetime measurements also measure the Raman scattering and if the coke species become larger, the coke species are more graphitic. These graphitic coke species are not fluorescence anymore and therefore the fluorescence lifetime will decrease, and the shape will be more like Raman scattering. The graphitization of the coke species is also shown in the Raman spectrum of the *in situ* and *ex situ* experiments, with an increasing G band.

For the *ex situ* experiments the RTR (%) is used for the determination of the G band, for the *in situ* experiment the RTR (%) can also be used. The calculation of the RTR (%) and the fit procedure is explained in chapter 3.8.

The results of the five different runs are shown in Figure 32. Figure 32A show the results of the fluorescence lifetime over time and Figure 32B, show the RTR (%) over time. These two graphs can be used to compare the five different coking experiments. As shown in Figure 32A the fluorescence lifetime of run 2 and 4 have a slow decrease of the fluorescence lifetime and the fluorescence lifetime only decreases 0.5 ns, from start to end. Figure 32B illustrates that the RTR (%) of these two runs has almost the same increase of RTR (%) over time and the maximum RTR (%) is around 8. Run 1, 3 and 5 shows in Figure 32A a stronger decrease of the fluorescence lifetime and Figure 32B shows that the RTR (%) of these three runs has a higher RTR (%), above 12%, compared to run 2 and 4. This means that these *in situ* measurements show that there is a correlation between the RTR (%) and the fluorescence lifetime of the coke species.

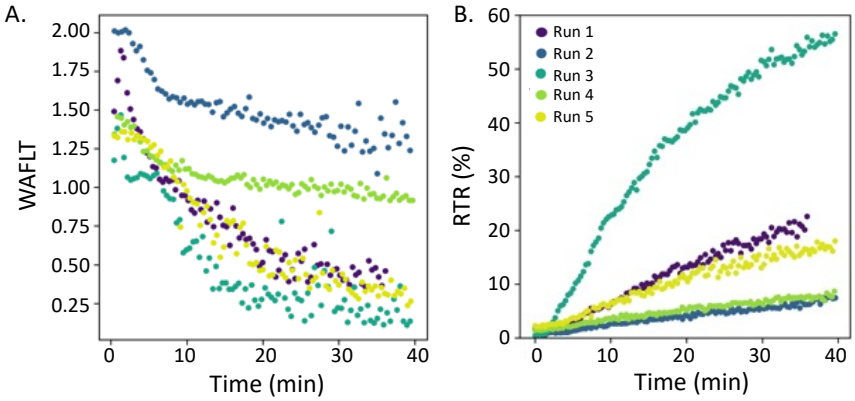

Figure 32: *Comparing the five in situ coking experiments. A. Weighted average of the fluorescence lifetime over time during the first 40 minutes. B. The RTR (%) over time during the first 40 minutes.*

The results of one of the regeneration experiments is shown in Figure 33. Figure 33A shows a few fluorescence lifetime measurements, 0, 2, 15 and 35 minutes. This shows that during the regeneration reaction the fluorescence lifetime first decreases and then increases. Figure 33B shows the heatmap of the first 15 minutes of the regeneration experiment. This heatmap shows the disappearing of the D and G band in the Raman spectrum. After 10 minutes there are no D and G bands in the Raman spectrum visible. Figure 33C shows a few Raman spectra, 0, 7, 10 and 20 minutes, this illustrates the disappearing of the D and G band in the Raman spectrum.

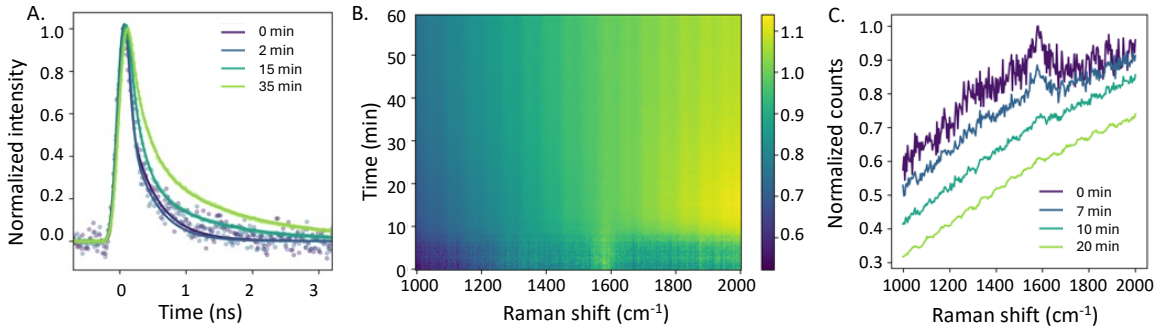

Figure 33: *Results of the in situ regeneration of Ecat. A. Fluorescence lifetime plot at 0, 2, 15 and 35 minutes. B. Heatmap of the Raman spectra (0-60 minutes). C. Raman spectra at 0, 7, 10, 20 minutes.*

The other three regeneration experiments show the same results as the first regeneration experiment. However, there is a difference in the time that the D and G bands are not visible in the Raman spectrum anymore. This is due to the different activities of the different catalyst particles.

4.4.3.2. Fcat

The *in situ* experiments are also performed with the fresh FCC particles, five different particles are used for the coking and the regeneration. In theory all the particles have similar activity, so the expectation is that the five runs show almost the same spectra and the same trends as the *ex situ* experiments.

The results of one coking experiment of a Fcat particle is shown in Figure 34. Figure 34A shows a few fluorescence lifetime plots, this graph shows that the fluorescence lifetime will first decrease, 3 and 8 minutes measurement, but after that the fluorescence lifetime will increase. This is also shown in Figure 34B, this plot shows the fluorescence lifetime over time, after around 20 minutes the fluorescence lifetime will increase. Comparing this to the results of the *ex situ* experiments, this is the same trend. Figure 34C shows the heatmap of the whole measurement, this graph shows that the G band appears in the Raman spectrum quickly. Figure 34D, shows a few Raman spectra and this shows that after four minutes the G band is visible in the Raman. However, the G band is not increasing during the whole measurement but after around 20-30 minutes the G band in decreasing. To compare the five different measurements Figure 34E can be used. This graph shows the RTR (%) over time, this graph shows the same trend as the individual Raman spectra (Figure 34D). Each particle has the same trend however there are some differences in the activity of the particles. This is due to the different sizes of the particles and therefore also the different amounts of active sites and the different activities.

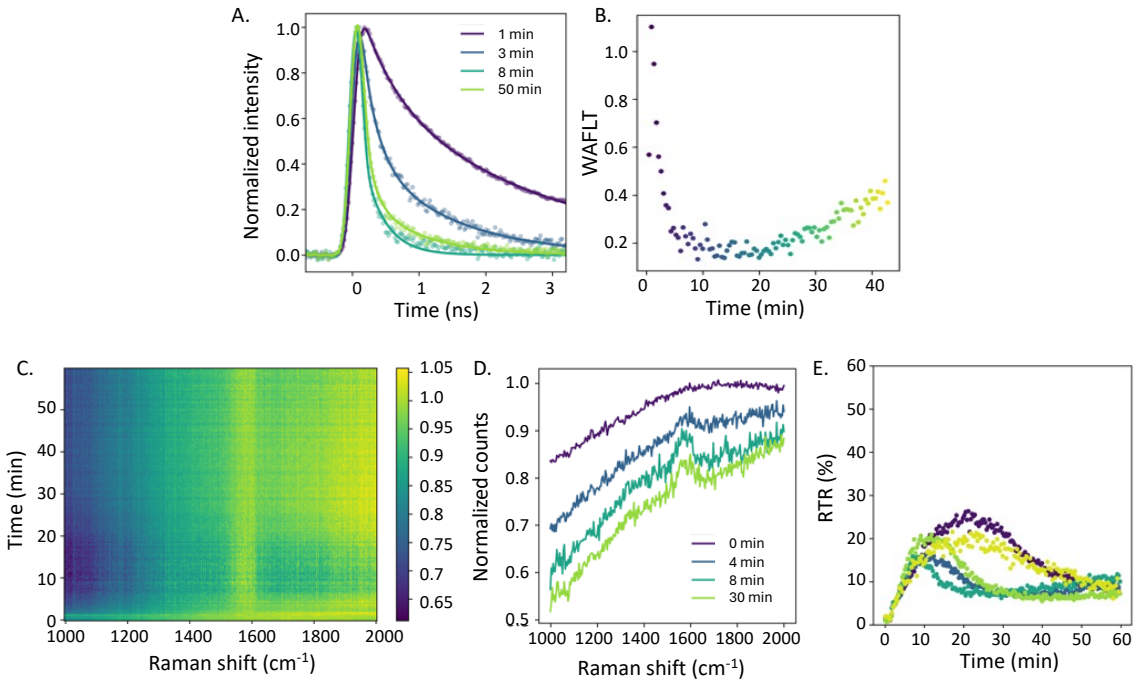

Figure 34: *Results of the in situ coking of Fcat. A. Fluorescence lifetime plots at 1, 3, 8 and 50 minutes. B. The weighted average of the fluorescence lifetime over time during the first 40 minutes. C. Heatmap of the Raman spectrum (0-60 minutes). D. Raman spectra at 0, 4, 8, 30 minutes. E. RTR (%) over time of the five different Fcat particles.*

The results of the *ex situ* experiments and the *in situ* show not completely the same trend for the fresh catalyst. Figure 35 shows the RTR (%) over time and the average fluorescence lifetime over time for the *ex situ* and the *in situ* experiments. Figure 35A and B shows the (average) fluorescence lifetime over time, these two plots show the same trend for both *ex situ* and *in situ* measurements.

Figure 35C shows an increase of the RTR (%) for the four different Fcat samples (*ex situ* measurements). However, Figure 35D shows that the *in situ* RTR (%) over time shows an increase followed by a decrease of the RTR (%) (*in situ* measurement). This means that the RTR (%) over time is not the same for the *ex situ* and *in situ* measurements. The reason for the different trend in the RTR (%) is not clear. Further investigation is needed to find a reason for this difference between the *ex situ* and *in situ* measurement.

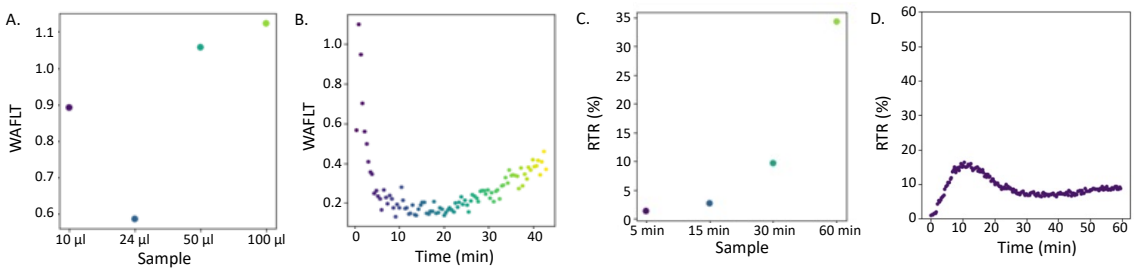

Figure 35: *Comparing the ex situ results vs in situ of the coking of Fcat. A. RTR (%) of the ex situ samples. B. RTR (%) over time during the in situ measurement. C. Weighted average of the fluorescence lifetime of the ex situ samples. D. Weighted average of the fluorescence lifetime over time during the in situ measurement.*

For all the five particles, the regeneration reaction is measured. Figure 36A shows a few fluorescence lifetime plots during the regeneration. This plot shows that the fluorescence lifetime increases during the regeneration. Figure 36B shows the heatmap of the whole measurement, in this graph it is difficult to see when the G band is not visible in the spectrum anymore. Therefore, Figure 36C shows a few Raman spectra, this graph shows the after 7 minutes the G band is not visible in the Raman spectrum anymore.

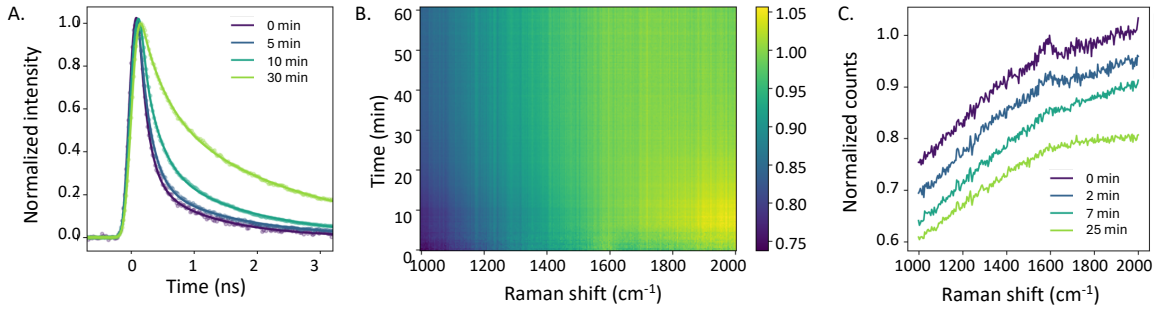

Figure 36: *Results of the in situ regeneration of Fcat. A. Fluorescence lifetime plot of in situ experiment regeneration of Fcat at 0, 2, 15 and 35 minutes. B. Heatmap of the Rama spectrum (0-60 minutes). C. Raman spectra at 0, 2, 7 and 25 minutes.*

5. Conclusions

This thesis describes the formation and identification of carbon deposits on fluid catalytic cracking catalyst particles. The FCC catalyst particles with different amounts coke species are successfully prepared with the hexane cracking reaction. Two sets of four samples are obtained with this reaction, one set with Ecat and the other set with Fcat. Both sets of samples are prepared with the same reaction conditions at a temperature of 550˚C and the same exposure times of hexane, 5, 15, 30 and 60 minutes, continuous flow. The third set of samples is prepared by Albemarle and different amounts of pulsed hexane are used to obtain different amount of coke species on the catalyst, 10, 24, 50 and 100 µl. The samples were characterized with TGA, confocal fluorescence microscopy and time-gated Raman spectroscopy.

The TGA results show that an increasing amount of hexane exposure results in an increasing amount of coke species on the catalyst. The Ecat samples (continuous flow), shows a weight loss between 0.4 and 0.7%, the weight loss of the Ecat samples (pulsed) are between 0.5 and 1.2%. The weight loss of the Fcat samples is between 1.3 and 6.3 %. The difference between the Ecat and the Fcat is the different activities for each Ecat particle. The Ecat particles have a lower activity because the particles already went through ±5000 cycles in the FCC reactor and therefore active sites are damaged.

The samples are analyzed with CFM, for the Ecat samples (continuous flow) a longer exposure time of hexane results in an increase of the intensity between 650-750 nm. Therefore, a longer exposure time of hexane results in relatively more larger coke species. The Ecat samples (pulsed) and the Fcat don't show the same trend. For the samples with the highest amount of hexane the intensity of the fluorescence signal decreases between 650-750 nm. The coke species on these samples are probably more graphitic and therefore show a very weak fluorescence signal.

Comparing the Raman spectra recorded with the time-gated Raman spectrometer and the conventional Raman spectrometer results in a lower background in the Raman spectrum recorded with the TGRS. However, a higher quality spectrum is recorded with the CCD. Therefore, it is not necessary to use TGRS for the Raman spectrum. Nevertheless, with the TGRS a fluorescence lifetime plot of the fluorescence signal can be obtained. This can give a lot of information about the nature of the coke species.

The *ex situ* experiments cannot be compared particle by particle due to the different activities of each particle. Therefore, the sample averages are used to find trends in the set of samples. The Ecat samples shows that a longer exposure time of hexane results in an increase of the average fluorescence lifetime followed by a decrease. The RTR (%) will increase with a longer exposure time of hexane. This means that more graphitic coke species will result in a higher RTR (%) and a lower fluorescence lifetime. The Fcat samples doesn't have the same trend, the average fluorescence lifetime will first decrease followed by an increase, with a longer exposure time of hexane. The RTR (%) will increase with a longer exposure time of hexane.

The *in situ* experiments of the Ecat sample show the same trend for the fluorescence lifetime and the RTR (%) as the *ex situ* experiments. The *in situ* experiments of the Fcat samples show the same trend for the fluorescence lifetime. However, the RTR (%) of the *in situ* experiments

doesn’t show the same trend as the *ex situ* experiments. The RTR (%) over time first increases and after around 20 minutes the RTR (%) decreases.

In conclusion, a method is developed for the investigation of the formation of the coke species. The results of the time-gated Raman spectrometer and the conventional Raman spectrometer give complementary information about the coke species.

6. Outlook

In this work, fluorescence signal was a challenging parameter, during the *in situ* experiments the intense fluorescence signal results in a saturated detector, therefore for some measurements it was not possible to use the measurements of the 0-3 minutes. For the Fcat samples the formation of the D/G bands starts after 2-3 minutes so the first measurements can give important information. This can be changed by using a laser with a different wavelength. A laser in UV range (244 nm) results in less fluorescence signal. Using a laser with a shorter wavelength can also result in the identification of small coke species. The fluorescence signal of small coke species (1-4 aromatic rings) cannot be obtained with the 532 nm laser.

Comparing the results of the fluorescence lifetime with the literature is challenging. A solution for this can be measuring PAH reference samples under the same conditions as the *ex situ* experiments. However, some PAHs are carcinogenic and therefore measuring these PAHs is also challenging. However, the fluorescence lifetime of these references can give information about the type of the coke species.

In literature the fluorescence lifetime of some PAHs is measured, and these reference samples are dissolved in a medium. The medium has a big influence on the fluorescence lifetime. Therefore, the references cannot be compared with the coke species on the catalyst. A solution can be dissolving the coke species in the same medium as the references. So, all the conditions of the coke species and the PAH references are the same and the fluorescence lifetime of the measurements can be compared.

Acknowledgements

I would like to express my gratitude to the people who helped me during my master thesis. First of all, I would like to thank Robin Vogel and Caroline Versluis for the daily supervision and guidance throughout my project. Especially Robin Vogel because your 'door' was always open for questions or other things I was struggling with. I also want to thank you for all the advice and feedback you gave on my poster and thesis. Secondly, I want to thank Sebastian Rejman for the TGA measurements. Lastly, I want to thank my first examiner Prof. dr. Eelco Vogt and my second examiner Dr. Matteo Monai.

References

(1) IPCC. *Global Warming of 1.5°C*; Cambridge University Press, 2022. https://doi.org/10.1017/9781009157940.

(2) WMO. *The Global Climate 2011-2020: A Decade of Accelerating Climate Change*.

(3) Edenhofer, Ottmar.; Pichs Madruga, R.; Sokona, Y.; United Nations Environment Programme.; World Meteorological Organization.; Intergovernmental Panel on Climate Change. Working Group III.; Potsdam-Institut für Klimafolgenforschung. *Renewable Energy Sources and Climate Change Mitigation : Special Report of the Intergovernmental Panel on Climate Change*; Cambridge University Press, 2012.

(4) Bennett, P.; Rossi, A.; Chair, P. B. *Bioenergy Chair of the IEA Bioenergy TCP in 2022 Under the IEA Framework for International Energy Technology Cooperation the Executive Committee of Each Technology Collaboration Programme (TCP) Must Produce an Annual Report for IEA Headquarters. The Contributions from the Task Leaders and Operating Agents to This Report Are Gratefully Acknowledged*.

(5) de Freitas, E. N.; Salgado, J. C. S.; Alnoch, R. C.; Contato, A. G.; Habermann, E.; Michelin, M.; Martínez, C. A.; Polizeli, M. de L. T. M. Challenges of Biomass Utilization for Bioenergy in a Climate Change Scenario. *Biology*. MDPI December 1, 2021. https://doi.org/10.3390/biology10121277.

(6) Vogt, E. T. C.; Weckhuysen, B. M. Fluid Catalytic Cracking: Recent Developments on the Grand Old Lady of Zeolite Catalysis. *Chemical Society Reviews*. Royal Society of Chemistry October 21, 2015, pp 7342–7370. https://doi.org/10.1039/c5cs00376h.

(7) Corma, A.; Huber, G. W.; Sauvanaud, L.; O'Connor, P. Processing Biomass-Derived Oxygenates in the Oil Refinery: Catalytic Cracking (FCC) Reaction Pathways and Role of Catalyst. *J Catal* **2007**, *247* (2), 307–327. https://doi.org/10.1016/j.jcat.2007.01.023.

(8) Pinheiro, C. I. C.; Fernandes, J. L.; Domingues, L.; Chambel, A. J. S.; Graça, I.; Oliveira, N. M. C.; Cerqueira, H. S.; Ribeiro, F. R. Fluid Catalytic Cracking (FCC) Process Modeling, Simulation, and Control. *Industrial and Engineering Chemistry Research*. January 11, 2012, pp 1–29. https://doi.org/10.1021/ie200743c.

(9) Chen, Y. M. Recent Advances in FCC Technology. *Powder Technol* **2006**, *163* (1–2), 2–8. https://doi.org/10.1016/j.powtec.2006.01.001.

(10) Bai, P.; Etim, U. J.; Yan, Z.; Mintova, S.; Zhang, Z.; Zhong, Z.; Gao, X. Fluid Catalytic Cracking Technology: Current Status and Recent Discoveries on Catalyst Contamination. *Catal Rev Sci Eng* **2019**, *61* (3), 333–405. https://doi.org/10.1080/01614940.2018.1549011.

(11) Ferreira, J. M. M.; Sousa-Aguiar, E. F.; Aranda, D. A. G. FCC Catalyst Accessibility—A Review. *Catalysts*. MDPI April 1, 2023. https://doi.org/10.3390/catal13040784.

(12) Meirer, F.; Kalirai, S.; Morris, D.; Soparawalla, S.; Liu, Y.; Mesu, G.; Andrews, J. C.; Weckhuysen, B. M. Life and Death of a Single Catalytic Cracking Particle. *Sci Adv* **2015**, *1* (3). https://doi.org/10.1126/sciadv.1400199.

(13) Ruiz-Martínez, J.; Buurmans, I. L. C.; Knowles, W. V.; Van Der Beek, D.; Bergwerff, J. A.; Vogt, E. T. C.; Weckhuysen, B. M. Microspectroscopic Insight into the Deactivation Process of Individual Cracking Catalyst Particles with Basic Sulfur Components. *Appl Catal A Gen* **2012**, *419–420*, 84–94. https://doi.org/10.1016/j.apcata.2012.01.016.

(14) Gholami, Z.; Gholami, F.; Tišler, Z.; Tomas, M.; Vakili, M. A Review on Production of Light Olefins via Fluid Catalytic Cracking. *Energies (Basel)* **2021**, *14* (4). https://doi.org/10.3390/en14041089.

(15) Jarullah, A. T.; Awad, N. A.; Mujtaba, I. M. Optimal Design and Operation of an Industrial Fluidized Catalytic Cracking Reactor. *Fuel* **2017**, *206*, 657–674. https://doi.org/10.1016/j.fuel.2017.05.092.
(16) Gupta, R.; Kumar, V.; Srivastava, V. K. *MODELING AND SIMULATION OF FLUID CATALYTIC CRACKING UNIT*.
(17) Veselý, M.; Valadian, R.; Merten Lohse, L.; Toepperwien, M.; Spiers, K.; Garrevoet, J.; Vogt, E. T. C.; Salditt, T.; Weckhuysen, B. M.; Meirer, F. 3-D X-Ray Nanotomography Reveals Different Carbon Deposition Mechanisms in a Single Catalyst Particle. *ChemCatChem* **2021**, *13* (10), 2494–2507. https://doi.org/10.1002/cctc.202100276.
(18) Buurmans, I. L. C.; Ruiz-Martínez, J.; Vana Leeuwen, S. L.; Vana Dera Beek, D.; Bergwerff, J. A.; Knowles, W. V.; Vogt, E. T. C.; Weckhuysen, B. M. Staining of Fluid-Catalytic-Cracking Catalysts: Localising Brønsted Acidity within a Single Catalyst Particle. *Chemistry - A European Journal* **2012**, *18* (4), 1094–1101. https://doi.org/10.1002/chem.201102949.
(19) Ma, W.; Liu, B.; Zhang, R.; Gu, T.; Ji, X.; Zhong, L.; Chen, G.; Ma, L.; Cheng, Z.; Li, X. Co-Upgrading of Raw Bio-Oil with Kitchen Waste Oil through Fluid Catalytic Cracking (FCC). *Appl Energy* **2018**, *217*, 233–240. https://doi.org/10.1016/j.apenergy.2018.02.036.
(20) Vogt, E. T. C.; Fu, D.; Weckhuysen, B. M. Carbon Deposit Analysis in Catalyst Deactivation, Regeneration, and Rejuvenation. *Angewandte Chemie - International Edition*. John Wiley and Sons Inc July 17, 2023. https://doi.org/10.1002/anie.202300319.
(21) Qian, K.; Tomczak, D. C.; Rakiewicz, E. F.; Harding, R. H.; Yaluris, G.; Cheng, W.-C.; Zhao, X.; Peters, A. W. *Coke Formation in the Fluid Catalytic Cracking Process by Combined Analytical Techniques*; 1997. https://pubs.acs.org/sharingguidelines.
(22) Selli, E.; Zaccaria, C.; Sena, F.; Tomasi, G.; Bidoglio, G. Application of Multi-Way Models to the Time-Resolved Fluorescence of Polycyclic Aromatic Hydrocarbons Mixtures in Water. *Water Res* **2004**, *38* (9), 2269–2276. https://doi.org/10.1016/j.watres.2004.01.042.
(23) Signorile, M.; Bonino, F.; Damin, A.; Bordiga, S. In Situ Resonant UV-Raman Spectroscopy of Polycyclic Aromatic Hydrocarbons. *Journal of Physical Chemistry C* **2015**, *119* (21), 11694–11698. https://doi.org/10.1021/acs.jpcc.5b02209.
(24) Rudnick, S. M.; Chen, R. F. *Laser-Induced Fluorescence of Pyrene and Other Polycyclic Aromatic Hydrocarbons (PAH) in Seawater*; 1998; Vol. 47.
(25) Meidinger, R. F.; St Germain, R. W.; Dohotariu, V.; Gillispie, G. D. *Fluorescence of Aromatic Hydrocarbons in Aqueous Solution N/A*; 1993.
(26) Cobb, W. T.; Mcgown, L. B. *On-Line Fluorescence Lifetime Detection for Chromatographic Peak Resolution*; 1990; Vol. 62. https://pubs.acs.org/sharingguidelines.
(27) Chen, J.; Huang, Y. W.; Zhao, Y. Characterization of Polycyclic Aromatic Hydrocarbons Using Raman and Surfaceenhanced Raman Spectroscopy. *Journal of Raman Spectroscopy* **2014**, *46* (1), 64–69. https://doi.org/10.1002/jrs.4612.
(28) Rieger, R.; Müllen, K. Forever Young: Polycyclic Aromatic Hydrocarbons as Model Cases for Structural and Optical Studies. *Journal of Physical Organic Chemistry*. April 2010, pp 315–325. https://doi.org/10.1002/poc.1644.

(29) Strickler, S. J.; Berg, R. A. Relationship between Absorption Intensity and Fluorescence Lifetime of Molecules. *J Chem Phys* **1962**, *37* (4), 814–822. https://doi.org/10.1063/1.1733166.
(30) *An Introduction to Fluorescence Spectroscopy*; 2000.
(31) Berezin, M. Y.; Achilefu, S. Fluorescence Lifetime Measurements and Biological Imaging. *Chem Rev* **2010**, *110* (5), 2641–2684. https://doi.org/10.1021/cr900343z.
(32) Datta, R.; Heaster, T. M.; Sharick, J. T.; Gillette, A. A.; Skala, M. C. Fluorescence Lifetime Imaging Microscopy: Fundamentals and Advances in Instrumentation, Analysis, and Applications. *J Biomed Opt* **2020**, *25* (07), 1. https://doi.org/10.1117/1.jbo.25.7.071203.
(33) Boens, N.; Qin, W.; Basarić, N.; Hofkens, J.; Ameloot, M.; Pouget, J.; Lefèvre, J. P.; Valeur, B.; Gratton, E.; VandeVen, M.; Silva, N. D.; Engelborghs, Y.; Willaert, K.; Sillen, A.; Rumbles, G.; Phillips, D.; Visser, A. J. W. G.; Van Hoek, A.; Lakowicz, J. R.; Malak, H.; Gryczynski, I.; Szabo, A. G.; Krajcarski, D. T.; Tamai, N.; Miura, A. Fluorescence Lifetime Standards for Time and Frequency Domain Fluorescence Spectroscopy. *Anal Chem* **2007**, *79* (5), 2137–2149. https://doi.org/10.1021/ac062160k.
(34) who. *II. RAMAN AND INFRARED SPECTROSCOPY*.
(35) Das, R. S.; Agrawal, Y. K. Raman Spectroscopy: Recent Advancements, Techniques and Applications. *Vibrational Spectroscopy*. November 2011, pp 163–176. https://doi.org/10.1016/j.vibspec.2011.08.003.
(36) IJETR042430.
(37) Cialla-May, D.; Schmitt, M.; Popp, J. Theoretical Principles of Raman Spectroscopy. *Physical Sciences Reviews*. De Gruyter June 1, 2019. https://doi.org/10.1515/psr-2017-0040.
(38) Cialla-May, D.; Schmitt, M.; Popp, J. Theoretical Principles of Raman Spectroscopy. *Physical Sciences Reviews*. De Gruyter June 1, 2019. https://doi.org/10.1515/psr-2017-0040.
(39) Kögler, M.; Heilala, B. Time-Gated Raman Spectroscopy – a Review. *Measurement Science and Technology*. IOP Publishing Ltd January 1, 2021. https://doi.org/10.1088/1361-6501/abb044.
(40) Vogel, R.; Prins, P. T.; Rabouw, F. T.; Weckhuysen, B. M. Operando Time-Gated Raman Spectroscopy of Solid Catalysts. *Catal Sci Technol* **2023**. https://doi.org/10.1039/d3cy00967j.
(41) Edinburgh Instruments. *How to Choose your Lasers for Raman Microscopy*.
(42) Novanta Photonics. *How to Choose a Raman Spectroscopy Laser*.
(43) Ferrari, A. C. Raman Spectroscopy of Graphene and Graphite: Disorder, Electron-Phonon Coupling, Doping and Nonadiabatic Effects. *Solid State Commun* **2007**, *143* (1–2), 47–57. https://doi.org/10.1016/j.ssc.2007.03.052.
(44) Bare, S. R.; Vila, F. D.; Charochak, M. E.; Prabhakar, S.; Bradley, W. J.; Jaye, C.; Fischer, D. A.; Hayashi, S. T.; Bradley, S. A.; Rehr, J. J. *Characterization of Coke on a Pt-Re/γ-Al2O3 Reforming Catalyst: An Experimental and Theoretical Study*.
(45) Zhang, C. C.; Hartlaub, S.; Petrovic, I.; Yilmaz, B. Raman Spectroscopy Characterization of Amorphous Coke Generated in Industrial Processes. *ACS Omega* **2022**, *7* (3), 2565–2570. https://doi.org/10.1021/acsomega.1c03456.
(46) Chen, K.; Zhang, H.; Ibrahim, U. K.; Xue, W. Y.; Liu, H.; Guo, A. The Quantitative Assessment of Coke Morphology Based on the Raman Spectroscopic Characterization

of Serial Petroleum Cokes. *Fuel* **2019**, *246*, 60–68. https://doi.org/10.1016/j.fuel.2019.02.096.
(47) Cloutis, E.; Szymanski, P.; Applin, D.; Goltz, D. Identification and Discrimination of Polycyclic Aromatic Hydrocarbons Using Raman Spectroscopy. *Icarus* **2016**, *274*, 211–230. https://doi.org/10.1016/j.icarus.2016.03.023.
(48) Signorile, M.; Bonino, F.; Damin, A.; Bordiga, S. In Situ Resonant UV-Raman Spectroscopy of Polycyclic Aromatic Hydrocarbons. *Journal of Physical Chemistry C* **2015**, *119* (21), 11694–11698. https://doi.org/10.1021/acs.jpcc.5b02209.
(49) Vogel, R.; Prins, P. T.; Rabouw, F. T.; Weckhuysen, B. M. Operando Time-Gated Raman Spectroscopy of Solid Catalysts. *Catal Sci Technol* **2023**. https://doi.org/10.1039/d3cy00967j.
(50) Chiuri, A.; Angelini, F. Fast Gating for Raman Spectroscopy. *Sensors*. MDPI AG April 2, 2021. https://doi.org/10.3390/s21082579.
(51) Jonkman, J.; Brown, C. M.; Wright, G. D.; Anderson, K. I.; North, A. J. Guidance for Quantitative Confocal Microscopy. *Nat Protoc* **2020**. https://doi.org/10.1038/s41596-020-0307-7.
(52) Elliott, A. D. Confocal Microscopy: Principles and Modern Practices. *Curr Protoc Cytom* **2020**, *92* (1). https://doi.org/10.1002/cpcy.68.
(53) Hepler, P. K.; Gunning, B. E. S. *Confocal Fluorescence Microscopy of Plant Cells*; 1998; Vol. 201.
(54) Van Vreeswijk, S. H. *Advanced Zeolite Characterisation Methods to Investigate the Methanol-to-Hydrocarbons Reaction*; 2020.
(55) McNamara, G.; Larson, J. M.; Davidson, M. W. *Spectral Imaging and Linear Unmixing*.
(56) Almas, Q.; Naeem, M. A.; Baldanza, M. A. S.; Solomon, J.; Kenvin, J. C.; Müller, C. R.; Teixeira Da Silva, V.; Jones, C. W.; Sievers, C. Transformations of FCC Catalysts and Carbonaceous Deposits during Repeated Reaction-Regeneration Cycles. *Catal Sci Technol* **2019**, *9* (24), 6977–6992. https://doi.org/10.1039/c9cy01680e.
(57) Liu, B.; Slocombe, D.; AlKinany, M.; AlMegren, H.; Wang, J.; Arden, J.; Vai, A.; Gonzalez-Cortes, S.; Xiao, T.; Kuznetsov, V.; Edwards, P. P. Advances in the Study of Coke Formation over Zeolite Catalysts in the Methanol-to-Hydrocarbon Process. *Appl Petrochem Res* **2016**, *6* (3), 209–215. https://doi.org/10.1007/s13203-016-0156-z.
(58) Kerssens, M. M.; Sprung, C.; Whiting, G. T.; Weckhuysen, B. M. Selective Staining of Zeolite Acidity: Recent Progress and Future Perspectives on Fluorescence Microscopy. *Microporous and Mesoporous Materials* **2014**, *189*, 136–143. https://doi.org/10.1016/j.micromeso.2013.10.015.
(59) Mores, D.; Kornatowski, J.; Olsbye, U.; Weckhuysen, B. M. Coke Formation during the Methanol-to-Olefin Conversion: In Situ Microspectroscopy on Individual H-ZSM-5 Crystals with Different Brønsted Acidity. *Chemistry - A European Journal* **2011**, *17* (10), 2874–2884. https://doi.org/10.1002/chem.201002624.
(60) *In-Situ Micro-Spectroscopy on Coke Formation Processes in Zeolites*.
(61) Ferrari, A. C.; Robertson, J. Resonant Raman Spectroscopy of Disordered, Amorphous, and Diamondlike Carbon. *Phys Rev B Condens Matter Mater Phys* **2001**, *64* (7). https://doi.org/10.1103/PhysRevB.64.075414.
(62) Maris, E. *Mapping Porous Solid Catalysts with Fluorescent Molecules and Nanoparticles*.

Appendix

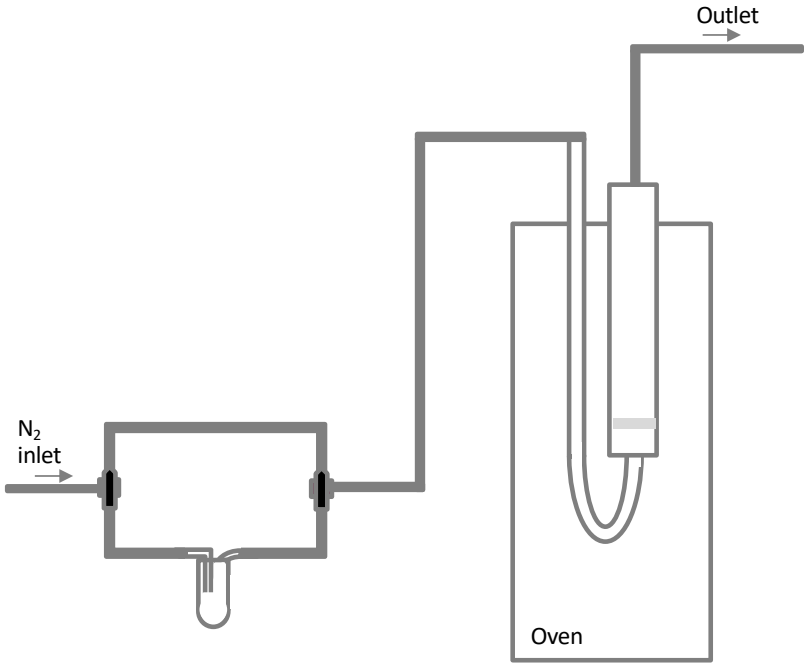

Figure 37: *Schematic view of the hexane cracking set-up used for the Ecat samples continuous flow and Fcat samples.*

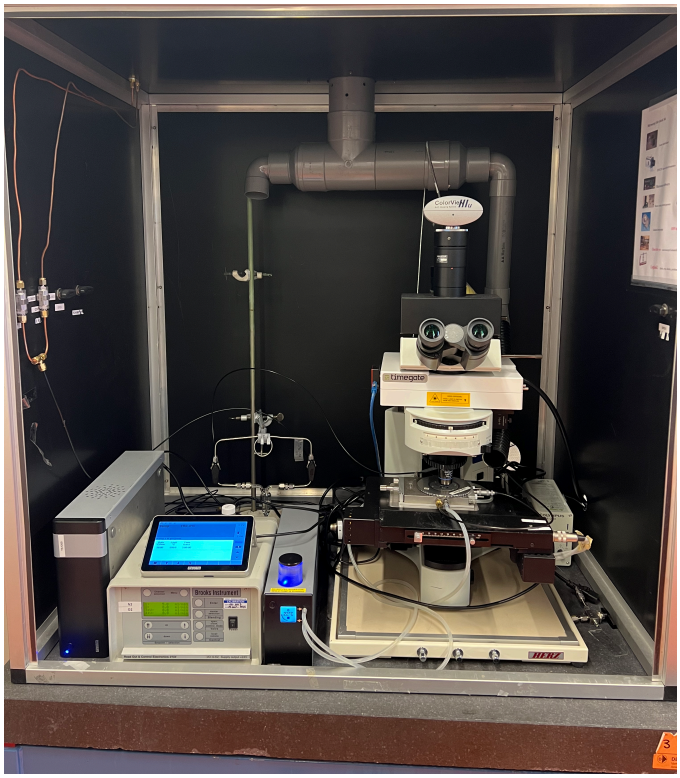

Figure 38: *Picture of the in situ set up.*

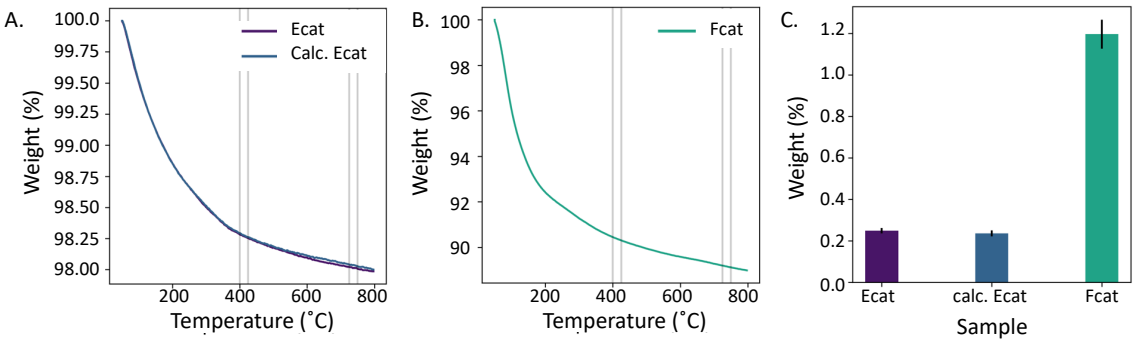

Figure 39: *Results of the TGA measurements of Ecat, calcined Ecat and Fcat. A. Raw data Ecat and calcined Ecat. B raw data of Fcat. C. Weight loss (%) of Ecat, calcined Ecat and Fcat.*